A Model for Predicting Narrow Tool Behavior under Dynamic Conditions

by

W. Christopher Swick

Thesis submitted to the Faculty of the

Virginia Polytechnic Institute and State University

in partial fulfillment of the requirements for the degree of

MASTER OF SCIENCE

in

Agricultural Engineering

APPROVED:

J. V. Perumpral, Chairman

J. S. Cundiff

G. Ulrich

October, 1984
Blacksburg, Virginia

A MODEL FOR PREDICTING NARROW TOOL BEHAVIOR UNDER DYNAMIC CONDITIONS

by

W. Christopher Swick

(ABSTRACT)

Most models available today for predicting the forces encountered by tillage tools apply to slow moving tools and do not take into account speed effects. However, most tillage operations are performed at speeds in the range of 2-8 km/h, and experimental studies show that tool forces increase significantly with tool speed.

This effort of developing a model for predicting the forces on narrow tools under dynamic conditions was carried out in three steps. First, a series of laboratory tests was conducted to determine the effect of shear rate on soil shear strength and soil-metal friction parameters. Second, a model was developed to include dynamic effects. Third, the model was verified experimentally under laboratory conditions.

Direct shear tests using a conventional shear box were conducted on an artificial soil at shear rates between 0.5 and 127 cm/min. Experimental results showed that for the

soil tested, the angle of internal friction, soil-metal friction angle, cohesion, and adhesion are independent of shear rate.

A soil-tillage tool interaction model developed for quasi-static soil failure was modified to include shear rate effects and accelerational force effects.

Experimental verification tests for the model were conducted under controlled conditions using an indoor soil bin facility. Tests were conducted with flat tines at speeds from 5.4 to 120 cm/s. The overall trend was for the model to underpredict the observed total tool force by 16 %. However, the model demonstrated that terms including accelerational force effects can account for a large portion of the increase in tool force observed to occur with an increase in tool speed.

ACKNOWLEDGEMENTS

The author would like to express his deep appreciation to the following:

To Dr. J. V. Perumpral for his guidance and patience during this study, and for serving as chairman of the graduate committee,

To Dr. J. S. Cundiff for his constant encouragement and serving on the graduate committee,

To Dr. G. Ulrich for his assistance in statistical design of the verification tests and analysis of experimental data,

To the Agricultural Engineering Department at Virginia Tech for financial assistance during the author's graduate program,

To his parents for many years of encouragement and support.

TABLE OF CONTENTS

LIST OF TABLES

LIST OF FIGURES

Chapter I

INTRODUCTION

The cultivation of fields by equipment is one of the oldest practices in agriculture. A relatively high level of development had been reached several hundred years ago, as the knife coulter, plowshare, and a crude form of the moldboard plow were in use as early as the eleventh century. Historically, however, advancements in tillage equipment and practices were by trial-and-error methods.

More recently, attempts have been made to describe the mechanics of the complex interaction between soil and tillage tools, with the ultimate goal of designing more efficient tillage tools. The first attempts in this connection were empirical in nature. Later, many employed semi-emperical or theoretical procedures for developing mathematical models to describe soil-tool interaction.

Most mathematical models available today are for tools moving at very low speeds. However, most tillage operations are performed at speeds in the range of 2-8 km/h, and experimental studies show that the forces encountered by tillage tools increase with tool speed. A better understanding of the effects of speed and other pertinent parameters on soil-tillage tool interaction is desirable for the design of more efficient tillage tools.

The objectives of this study were:

1. To determine the effect of shear rate on soil strength and soil-metal friction parameters.
2. To modify a quasi-static model to include speed effects.
3. To experimentally verify the dynamic model through laboratory tests.

Chapter II

LITERATURE REVIEW

Soil dynamics, as described by Gill and Vanden Berg (1968), is a phase of soil science and mechanics concerned with soil in motion, and may be defined as the relation between forces applied to soil and the resultant soil reaction. Soil dynamics associated with soil-tillage tool interaction, as a rule, involves soil loaded to the point of failure with masses of soil being displaced by the tool. Except where stated otherwise, the investigations mentioned here assume that soil fails along a surface according to the Mohr-Coulomb failure criterion:

$$\tau = c + (\sigma)\tan(\phi) \quad \text{......(1)}$$

and the reaction at soil-metal interfaces follows a similar criterion:

$$\tau' = A_d + (\sigma')\tan(\delta) \quad \text{......(2)}$$

where: τ = shear stress at the failure plane, N/cm^2

c = soil cohesion, N/cm^2

σ = normal stress at the failure plane, N/cm^2

ϕ = angle of internal friction, degrees

τ' = shear stress at the soil-metal interface, N/cm^2

A_d = soil-metal adhesion, N/cm^2

σ' = normal stress at the soil-metal interface, N/cm^2

δ = soil-metal friction angle, degrees

2.1 TWO-DIMENSIONAL MODELS.

Soehne (1956) studied the action of simple inclined tools operating in damp sand and developed four behavioral equations to describe the tillage tool action. These equations accounted for soil-metal friction, soil shear failure, cutting resistance, and the accelerational force for each block of soil. Adhesional forces were neglected. The mechanics Soehne developed was two-dimensional and did not consider the forces on the sides of the soil block. Thus, as with other two-dimensional models, the analysis was theoretically correct only for very wide tools.

Experimental verification by Soehne showed marginal agreement between observed and calculated draft force. Possible reasons for disagreement were that frictional forces on the sides of the tool and forces created by soil contacting the standards supporting the tool were not eliminated.

Rowe and Barnes (1961) refined the model by Soehne to include the effect of adhesion. They assumed that soil-metal

friction is independent of speed while soil shear strength varies with speed. Series of tests were conducted to determine the soil strength at several shear rates. Comparison of measured and calculated draft using the varying shear strength showed reasonable agreement. From the study, Rowe and Barnes concluded that the accelerational effect on the draft force is relatively small. The increase in draft force from increase in tool speed was attributed to higher shearing strength of the soil at higher shear rate.

Osman (1964) developed a model based on Passive Earth Pressure Theory to describe the mechanics of soil cutting by wide tools. This model was based on the graphical method developed by Ohde (1938) and described by Terzaghi (1943). Ohde proposed that the failure surface be a combination of a logarithmic spiral and a straight line inclined at $(45-\phi/2)$ degrees to the horizontal, and he used a trial and error procedure to select the actual failure wedge. Osman also used a trial and error procedure, but he developed a numerical method to replace Ohde's more complex graphical approach.

Tests were conducted for a variety of rake angles and tool surface finishes in dry sand, wet sand, and clay. The model solution gave reasonable agreement with measured forces for all experiments. Osman also found that soil-metal

friction angle had an important effect on draft, particularly for near-vertical tools.

O'Callaghan and Farrelly (1964) used classical soil mechanics theories in their investigation of soil failure in front of loaded vertical tines. Two distinct modes of soil rupture were identified and models for each mode were suggested. Tines with a depth-width ratio less than 0.6 were classified as "shallow" tools and were considered to act as retaining walls. Tines with a ratio greater than 0.6 were classified as "deep" tools and were considered to act as a footing. Rupture by shallow tines was considered two-dimensional in a vertical plane, and the failure surface was assumed to be similar to the one used by Osman (1964). Rupture by deep tines was considered two-dimensional in a horizontal plane and was modeled as failure caused by a vertical footing in the manner presented by Pradtl (1920) and discussed by Terzaghi (1943). Tines with widths of 51 to 122 mm were tested at depths between 25 and 178 mm in sandy loams and clay loams. Agreement between measured and calculated draft was reasonable. The observed critical depth-width ratio separating the vertical and horizontal failure regimes was found to vary between 0.5 and 1.

Siemens et al. (1965) investigated the mechanics of soil-tool interaction. Included in the study were measure-

ments of failure wedges and forces acting on plane tines. One of the assumptions of this study was that the failure wedge for rake angles between 90 and 70 degrees had a curved failure surface, similar to the one in front of a retaining wall with a rough surface. For tool angles less than 70 degrees, the failure surface was assumed to be a plane at an angle of $(45-\phi/2)$ degrees to the horizontal.

Tools with widths of 51 to 122 mm and rake angles from 15 to 90 degrees were tested, all at a depth of 51 mm in an artificial soil. Tool speeds ranged from 22.4 to 89.4 cm/s. Draft force was found to increase with tool speed, however, the calculated force due to acceleration, as predicted by the equation derived by Soehne (1956), was not nearly large enough to explain the difference in draft between the tests at 22.4 and 89.4 cm/s. Comparison of measured and calculated draft force showed that the model tended to underpredict tool forces. A build-up of soil was noticed to form near the bottom of the tools, and the location of the resultant force was found to be much lower on the tools than predicted by theory, suggesting that higher levels of soil compression took place near the bottom of the tools.

Hettiaratchi et al. (1966) developed a procedure for calculating the tool force encountered in two-dimensional soil failure. The equation developed was similar to the one originally proposed by Reece (1965) and can be expressed as:

$$P = \gamma D^2 N_\gamma + cDN_c + A_d DN_a + qDN_q \quad \ldots\ldots\ldots\ldots\ldots\ldots\ldots\ldots (3)$$

where: γ = unit weight of soil, N/cm^3

β = angle tool makes with the horizontal, degrees

D = depth of tool, cm

q = surcharge pressure at soil surface, N/cm^2

N_γ, N_c, N_a, N_q are dimensionless coefficients.

The four terms represented the gravitational, cohesive, adhesive, and surcharge components of the soil reaction per unit width of tool. The dimensionless coefficients associated with each of the four components were functions of ϕ, δ, and the geometry of the loaded interface. A set of 8 charts was developed to obtain values of the four coefficients in the equation. Inertial effects were neglected and hence the equation was valid only for slow moving tools. A curved failure surface was assumed. Tool angles considered ranged between $(45-\phi/2)$ and $(180-\phi)$ degrees. Tool forces predicted by the model showed close agreement with those calculated by Ohde's (1938) graphical method, however no experimental verification was given.

A basic limitation of the model was that for generating the dimensionless coefficients, it was assumed that:

$$c/\gamma D = A_d/\gamma D = q/\gamma D = 1 \quad \ldots\ldots\ldots\ldots\ldots\ldots\ldots\ldots (4)$$

Hettiaratchi et al. noted that for values of $c/\gamma D$ and $A_d/\gamma D$ less than one, the error induced by using the graphs was never more than 5 %. However, for values of the same terms greater than one, in conjunction with large values of ϕ, the error could be as high as 20 %.

Hettiaratchi and Reece (1974) reported refinements to their two-dimensional model to overcome some of its previous limitations. The new model considered tool angles from 5 to 170 degrees and treated adhesional effects differently. To relax the assumption that $c/\gamma D=A_d/\gamma D=1$, the following terms were used:

$$S_c = c/\gamma D \quad \text{.....(5)}$$

$$S_q = q/\gamma D \quad \text{.....(6)}$$

$$S = S_c + S_q \quad \text{.....(7)}$$

where: S_c, S_q are dimensionless numbers.

S is a dimensionless soil scale index.

The final form of the resulting soil resistance equation was:

$$P = \gamma D^2 K_\gamma + cDK_{ca} + qDK_q - (\gamma DK_s \exp(-S)) \quad \text{.....(8)}$$

where: K_γ, K_{ca}, K_q, K_s are dimensionless coefficients.

Again a set of 8 charts was given for determining the dimensionless coefficients. The model was not experimentally verified.

2.2 THREE-DIMENSIONAL MODELS.

Payne (1956) made a detailed analysis of the relationship between the mechanical properties of soil and the mechanics of soil failure around vertical tines. In this laboratory and field study, different soils ranging from sand to clay were considered. The investigation primarily dealt with the three-dimensional failure around "narrow" tines with depth-width ratios greater than 1:1. The maximum ratio considered was 25:1. Payne ignored accelerational effects and rate effects on soil strength and soil-metal friction, considering them to be small.

Payne used Passive Earth Pressure Theory to describe the soil failure in front of the vertical tines. He observed that a wedge of triangular cross-section in the horizontal plane formed on the face of all tines. The wedge moved slowly up the tool face due to the vertical component of the forces acting on the logarithmically-curved failure surface assumed to develop forward from the base of the tool. Payne considered this vertical soil wedge to act as a retaining wall, pushing crescents of soil up and to the sides, ahead

of the tool. Thus, soil forces were analyzed assuming that the soil crescents were formed to the sides under passive earth pressure, being displaced by a wedge-shaped retaining wall with friction angle and adhesion equal to the soil internal friction angle and soil cohesion, respectively. Draft force on the tool was determined by summing the resulting forces on the triangular soil wedge in the vertical and horizontal directions. The major limitation of the mechanics developed is that the solution proposed for the forces under the assumed failure pattern is not presented in a readily usable form.

Payne and Tanner (1959) investigated the relationship between the rake angle and the performance of flat tines. Four tine widths ranging from 21 to 101 mm were used at a constant depth of 152 mm with rake angle varying from 20 to 160 degrees with the horizontal. During field tests in a variety of soils, vertical and horizontal forces and failure patterns were determined. The crescent-shaped failure pattern observed by Payne (1956) for vertical tines was found to be elongated for rake angles less than 90 degrees and shortened for angles greater than 90 degrees. The triangular soil wedge found by Payne (1956) was observed to move up the face of tools with rake angles of 20 to 104 degrees, and to form in a stationary position at the bottom of tools with

rake angles greater than this. Draft was relatively insensitive to rake angle betweem 20 and 50 degrees, but increased rapidly for greater angles.

Hettiaratchi and Reece (1967) modified their two-dimensional model (Hettiaratchi et al., 1966) to include three-dimensional soil failure for tool angles in the range of 0 to 90 degress. The assumed shape of the soil wedge in front of the tool depended on the tool depth. Two failure regimes were used to develop the model and were considered to be the two orthogonal planar components of the three-dimensional solution. The vertical failure regime was envisioned to cause "forward failure" ahead of the tool analogous to that in the two-dimensional model. Thus equation (3) was used to determine this component of the total soil reaction. The horizontal failure regime was envisioned to produce "sideways failure" around the tool, creating the force component:

$$P_s = [\gamma(D+q/\gamma)^2 wN_{s\gamma}+cwDN_{sc}]K_a \quad \ldots\ldots\ldots\ldots\ldots\ldots\ldots\ldots\ldots\ldots(9)$$

where: $N_{s\gamma}$, N_{sc}, K_a are dimensionless coefficients.

Two charts were developed for determining the three coefficients. Comparison of model predictions with test results showed that the model overpredicted draft for near-vertical tools with small depth-width ratios.

Godwin and Spoor (1977) developed a model to predict draft force on tines with a wide range of depth to width ratios. The model was based on the size and shape of the failure wedge in front of the tools. Tests were conducted in a glass-sided box to observe soil failure ahead of moving tines of various widths and rake angles. A compacted soil wedge was found to form on the face of all tines. Ahead of this wedge two modes of failure were observed. With tines of small depth-width ratio, soil moved forward and upward along the entire depth of the tine with a definite shear plane developing forward from the base of the tine (crescent failure). As the depth-width ratio increased, soil below a certain depth, called the critical depth, appeared to move forward with no definite shear plane being formed (lateral failure).

The three-dimensional crescent failure ahead of tools for depths less than or equal to the critical depth, was considered to have three sections. The first section directly in front of the tool, was assumed to have the same width as the tool. The passive force on this wedge was calculated using the two-dimensional model developed by Hettiaratchi et al. (1966). Side crescents were envisioned to occur on both sides of the center wedge. The top view of each side crescent was circular in shape. The passive force on each side

crescent was calculated by applying the Hettiaratchi et al. (1966) model to a differential element and integrating over the entire crescent. For tools operating at depths greater than the critical depth, two-dimensional lateral failure in a horizontal plane was assumed for the portion of the soil below the critical depth. The passive earth pressure developed by the lateral failure was determined using the method developed for footings by Meyerhof (1951). Verification tests were conducted at a constant speed of 56 cm/s. Comparison of calculated and measured forces showed reasonable agreement.

McKyes and Ali (1977) developed a three-dimensional model for predicting the horizontal draft force on simple tines and the volume of soil disturbed around the tines. The shape of the failure wedge considered was similar to the one considered by Godwin and Spoor (1977) with one exception. McKyes and Ali assumed a straight line failure surface instead of a logarithmic spiral surface. Included in the model were effects of soil density, soil internal friction angle, soil-metal friction angle, soil cohesion, and surface surcharge pressure, but not the effect of adhesion at the soil-tool interface. The forces created by these effects were considered to create a condition of equilibrium. Forces were summed in the horizontal and vertical directions and

solved for the draft force. The final equation contained two unknowns, the draft force and the angle that the rupture plane made with the horizontal. The draft force was minimized with respect to the rupture angle.

McKyes and Ali (1977) and McKyes (1978) compared the model predictions with test results and concluded that the model gave reasonable predictions of draft force and volume of soil disturbed.

2.3 INERTIAL EFFECTS AND DYNAMIC SOIL PROPERTIES.

Wismer and Luth (1972) investigated rate effects in soil cutting and presented their findings on inertial effects and shear strength. In their analysis of inertial effects for two-dimensional flow of soil over an inclined tool, they used the equation derived by Soehne (1956) to predict the inertial force. Laboratory tests were conducted with a segmented blade inclined at an angle of 30 degrees such that only the forces due to a 126 mm wide center section were measured. Results from blade tests in air dry sand showed that the inertial force prediction accounted for the increase in horizontal and vertical forces at speeds up to 255 cm/s. However, tests in a Decatur silty clay loam showed that calculated inertial force accounted for only about 40 % of the force increase over the same speed range.

The shear strength studies by Wismer and Luth involved moving cone penetrometers of two diameters horizontally through saturated clay soils at various speeds. They used a dimensional analysis scheme similar to that of Turnage and Frietag (1970) to relate actual cone size and velocity to those of the standard cone penetrometer and standard penetration rate. Plots of cone index vs. penetration rate were found to have the same shape as draft vs. tool speed for saturated clays, that of a decaying exponential curve.

Stafford (1979) evaluated the performance of tines in terms of soil forces and soil failure over a wide range of soil moisture contents and a thousand-fold range of speed in two soils. One soil contained 60 % clay, while the other contained 60 % sand. The tools tested were 4 cm wide and operated at a depth of 15 cm with rake angles of 45 and 90 degrees. Test speeds ranged from 5 mm/s to 5.5 m/s. Stafford found that the performance fell into one of two regimes determined by the soil moisture content. The transition between the two regimes occured slightly below the plastic limit of the soil.

At low moisture content, draft vs. speed data was fitted with polynomial curves, and at high moisture content the data was fitted with decaying expontial curves for both the clay and sandy soils. The fit of all curves was statistically significant at the 5 % level.

The two-dimensional model of Hettiaratchi et al. (1966) and the three-dimensional model of Hettiaratchi and Reece (1967) were used by Stafford in a comparison of calculated and measured draft at near-zero speed. The predictions from the three-dimensional model were at least an order of magnitude too high. However, the two-dimensional model gave good prediction, especially at the lower moisture contents. It was concluded that the overpredictions of the three-dimensional model were due to too large a contribution from the side failure zone.

Aref et al. (1975) used the method of deformation energy partition to gain insight into the variation of soil strength properties with changes in speed of loading or deformation. They conducted confined and unconfined compression tests on a clay loam soil at axial strain rates of 0.018 min^{-1} and 0.254 min^{-1}. They found that the energy needed to compress the soil was not affected by strain rate, but the peak stress was affected.

Flenniken et al. (1977) studied the unconfined compressive strength of soils at compression rates up to 480 cm/s. Most of the observed increase in shear strength occured below a deformation speed of 90 cm/s (axial strain of 10 s^{-1}). The increase in strength with increase in strain rate of five soils tested seemed dependent on the clay content, den-

sity, and structure or condition of the soil. Investigations on two of the soils showed that the increase in peak stress was effective in accounting for additional draft force observed with increasing tool speed. Also it was found that the energy to peak stress was linearly related to strain rate.

Rowe and Barnes (1961) investigated the effect of shear rate on shear strength for four different soils in developing their soil-tool interaction model. Shearing resistance was measured with a torsional device, with shear rates varying from 1.9 to 69 cm/s. The change in shear strength was small for sand but became progressively larger for soils of higher clay content. The increase in draft force they observed with increasing tool speed, was attributed to the increase in shearing strength of the soil due to the higher shear rate.

Stafford and Tanner (1983a,1983b) studied the effect of shear rate on soil strength and soil-metal friction. The soils studied were the same as those used by Stafford (1979). A torsional shear device was built for the tests, able to shear soil in the range equivalent to 0.15 to 500 cm/s. The rotational speed could be continually varied from 0.1 to 40 revolutions per second. Soil cohesion and soil-metal friction angle were found to vary logarithmically with

shear rate for a wide range of moisture content in both soils. Soil internal frictional angle was found independent of shear rate while no general relationship was found between adhesion and shear rate. Residual shear strength did not vary in a consistent manner.

From the literature reviewed in this chapter, it appears that the forces encountered by tillage tools moving at very low speeds can be predicted with reasonable accuracy. However, there are few models available for predicting the forces encountered by tools operating at field speeds (2-8 km/h). Those investigators that are developing models for predicting soil-tool interaction under dynamic conditions appear to be concentrating their efforts on including the effects of accelerational forces and dynamic soil strength properties. The present study was begun with this in mind.

Chapter III

PROCEDURES

Experimental studies have shown that the forces encountered by tillage tools increase in magnitude as a function of tool speed. The model developed in this study for predicting the forces on tools under dynamic conditions is based on a hypothesis that a large portion of the increase in tool forces can be attributed to the following two phenomena:

1. soil shear strength and soil-metal friction increase with increasing shear rate, and
2. the force required to accelerate the soil from a state of rest to a certain velocity depends on tool speed and soil failure geometry.

The above hypothesis was tested in three steps for tines working in an artificial soil. First, a series of laboratory tests was conducted to determine the effect of shear rate on soil shear strength and soil-metal friction parameters. Second, a soil-tillage tool interaction model developed for quasi-static soil failure was modified to include the shear rate effects and accelerational force effects. Third, the model was verified experimentally under laboratory conditions. The procedure involved in each step is discussed in this chapter.

3.1 SHEAR RATE EFFECTS ON SOIL STRENGTH AND FRICTION PARAMETERS.

3.1.1 Laboratory test facility.

A square shear box used for conventional direct shear tests was used to determine the effect of shear rate on soil strength and soil-metal friction parameters. An overall view of the test facility is shown in Figure 1. It includes an Instron test machine, the shear box on a stand, and instrumentation for recording the experimental data.

An Instron test machine, Model TM-S + 3111, was used to displace the upper half of the shear box at different rates while recording force and displacement data. The Instron machine was capable of providing test speeds in the range of 0.5-127.0 cm/min. A stand which could be fixed rigidly to the base of the Instron was constructed and mounted to hold the shear box in place. A cable and pulley system was used to translate the vertical displacement of the Instron crosshead to horizontal displacement at the shear box. The cable was selected carefully so that elongation under the loads encountered in this study was negligible.

The chart speed and crosshead speed on the Instron machine were synchronized so that the strip chart recorder provided plots of horizontal pull as a function of crosshead displacement. Since some movement of the crosshead was expected to fully tighten the cable prior to displacing the

Figure 1 An overall view of the experimental set up used to determine the effect of shear rate on soil strength and soil-metal friction parameters.

shear box, a Daytronic Model DS500 Linear Variance Displacement Tranducer (LVDT) was mounted on the stand to monitor the actual displacement of the shear box. A Sanborn Model 592-300 converter was used to provide excitation to the transducer and a Gould Model 220 strip chart recorder was used to record the transducer output. The LVDT output was used to determine the shear box displacement at maximum shear resistance and to check whether or not shear box displacement was at a constant rate. The ultimate strengths of the soil and the soil-metal interface occurred at shear box displacements of 7.5 to 10.0 mm. At the same time, the top half of the shear box reached a constant rate of displacement within 1.2 mm. Thus it was concluded that the portion of the shear box displacement for which displacement rate was not constant was insignificant, and that any force necessary to accelerate the mass of the shear box with the sample up to the desired constant rate, occured well before the peak shear resistance.

3.1.2 Test procedures.

For determining the effects of shear rate on soil strength parameters, soil samples were prepared in the shear box. The samples were prepared by placing layers of 0.4 cm loose soil in the box and compacting them to a density equal

to that selected for the soil bin tests. A normal load was then placed on the soil sample through a plate by hanging dead weights on a vertical hanger. The top crossbar of the hanger rested on the center of the plate. The test was then conducted by disaplacing the upper half of the shear box at a predetermined rate while holding the bottom half stationary. During each test, displacement and horizontal pull were recorded continuously.

Tests for determining the rate effects on soil-metal friction parameters were the same with one exception. For these tests, instead of soil, a square steel plate constructed of the same stock used for construction of the tines was placed in the bottom half of the shear box. The top half of the box contained the soil sample. As in the direct shear tests, a normal load was applied and half of the shear box was displaced, recording the pull and the displacement simultaneously.

Three shear rates were used during testing to observe the effects of shear rate on strength and soil-metal friction. They were 0.5, 50.8, and 127.0 cm/min, spanning the total range available on the Instron machine. Results of preliminary soil bin tests were used to estimate the average normal pressures which occured at the soil rupture surfaces and soil-tool interface. The normal pressures thus selected for

the shear strength tests were 0.77, 1.41, and 1.97 N/cm^2. The normal pressures used for determining the soil-metal friction were 2.70, 7.46, and 11.8 N/cm^2.

Force-displacement data collected during tests was used to determine the maximum force encountered during tests. Using this data, maximum shear stress vs. normal stress plots were made for each shear rate tested.

Least squares regression equations in the form of equation (1) were fitted to the results of the soil shear strength tests to determine estimates of soil cohesion and angle of internal friction. Similarly, equation (2) was fitted to the soil-metal friction test results to obtain the soil-metal adhesion and soil-metal friction angle. The results which will be discussed later in more detail showed that for the artificial soil, the soil cohesion factor, soil internal friction angle, soil-metal adhesion, and soil-metal friction angle were independent of shear rate.

3.2 DEVELOPMENT OF DYNAMIC MODEL.

A soil-tool interaction model developed earlier (Grisso, 1980; Perumpral et al., 1983) was chosen to provide the basis for the dynamic soil-tool interaction model. This quasi-static model was chosen because of its simplicity as well as its prediction capabilties under quasi-static conditions.

A brief description of the quasi-static model and alterations made to include the dynamic effect are discussed in this section.

3.2.1 Quasi-static soil-tool model.

The quasi-static model developed to predict narrow tillage tool behavior in soils took into consideration a three-dimensional failure wedge (Figure 2) in front of a moving narrow tool. The model developed is based on several assumptions which are not repeated here since they are listed in Grisso (1980) and Perumpral et al. (1983). However, the most important of all the assumptions is that the wedge shown in Figure 2 could be idealized by replacing the side wedges with a set of forces on either side of the center wedge. The dimensions of the idealized wedge and the forces acting on the wedge are shown in Figures 3 and 4 respectively. Another simplifying assumption involved in the idealization included considering the curved rupture surface as a straight plane surface (face bcfe in Figure 4).

The three forces acting on either side of the idealized wedge, on planes abc and def, represented the contribution of the side wedges. On each plane, this included one force vector normal to the plane and the other two on the plane. An expression for the normal force is:

$$R = \gamma K_o z A \qquad (10)$$

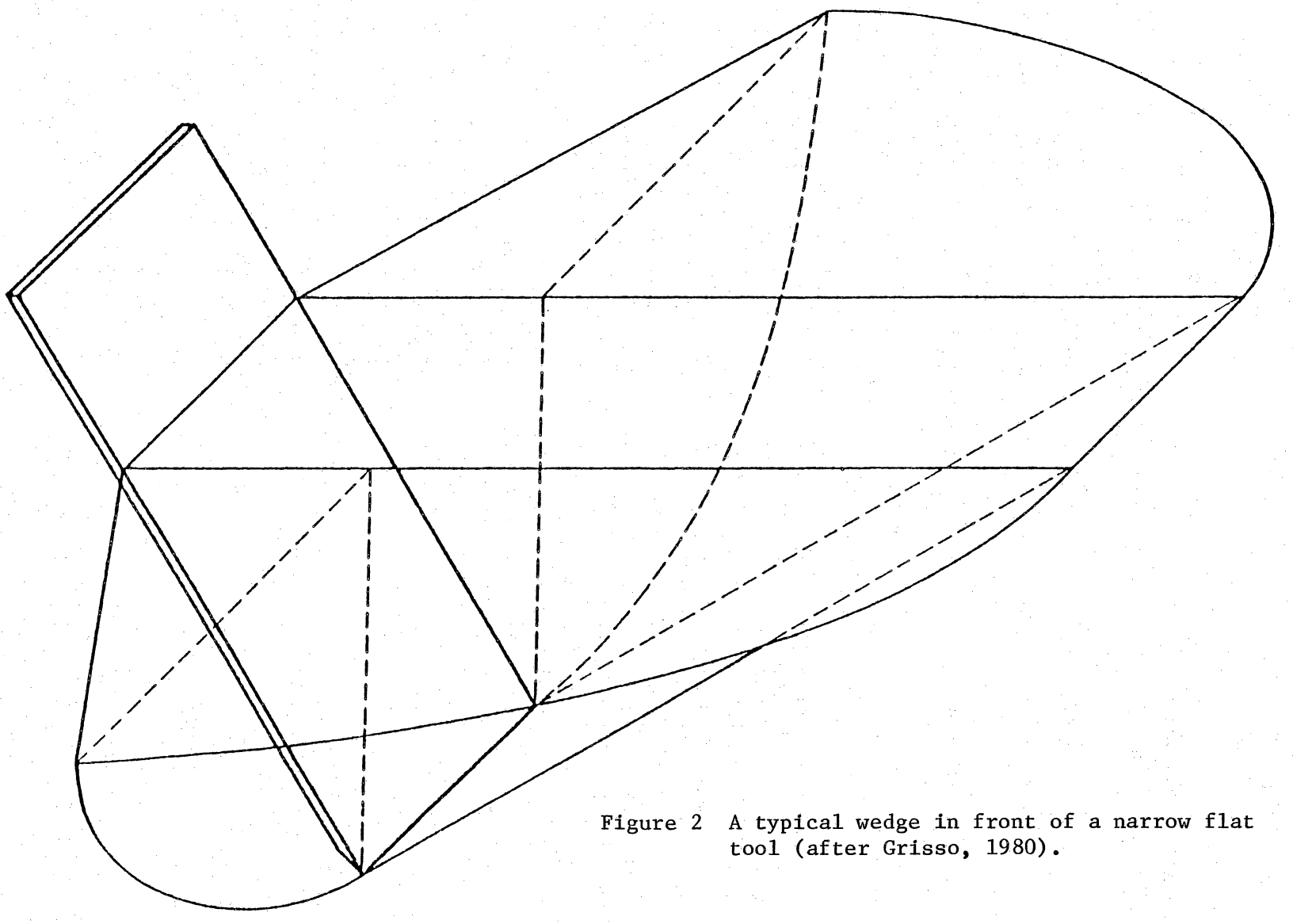

Figure 2 A typical wedge in front of a narrow flat tool (after Grisso, 1980).

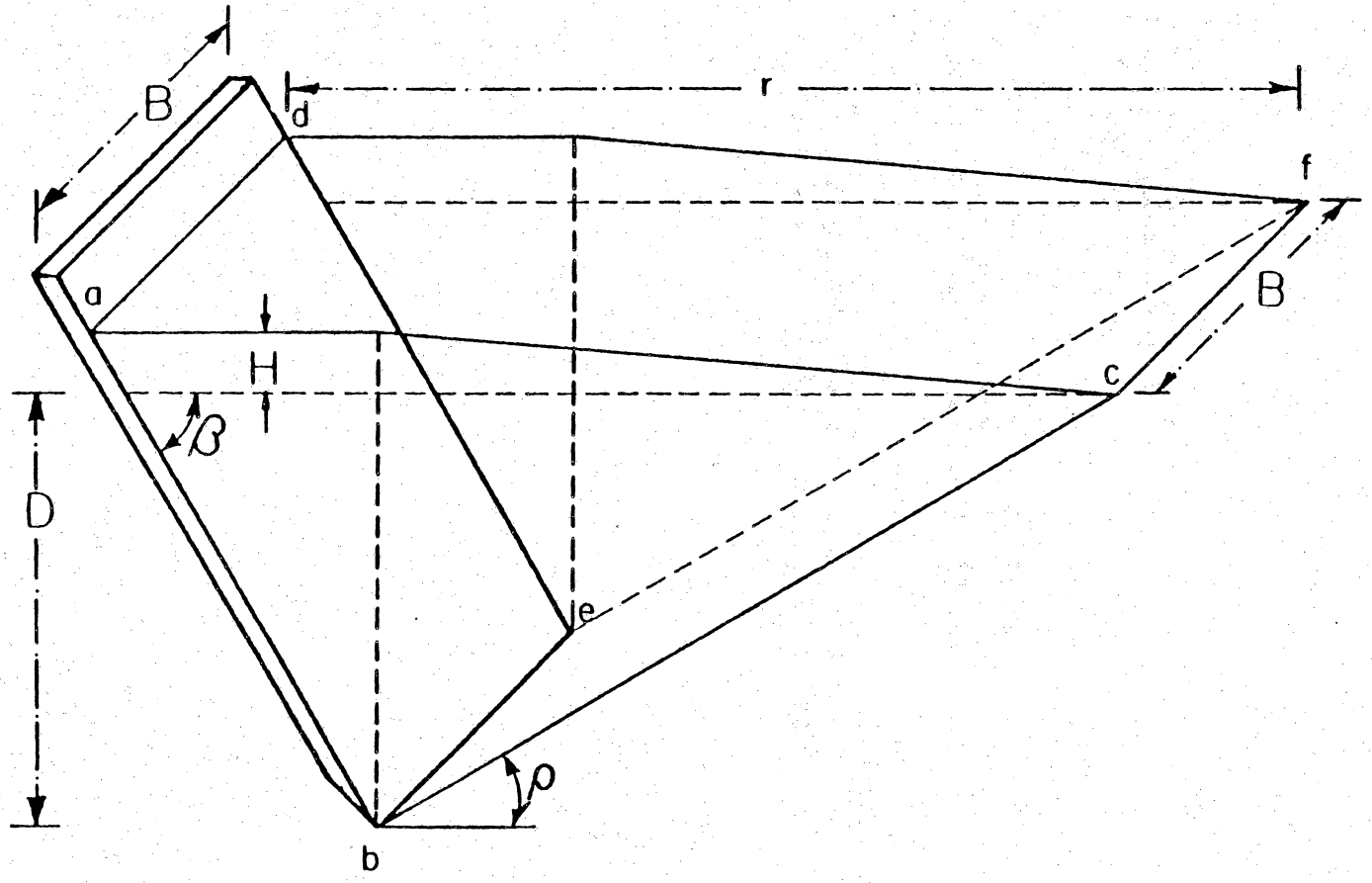

Figure 3 Geometric boundaries of an idealized failure wedge considered for the quasi-static model (after Grisso, 1980).

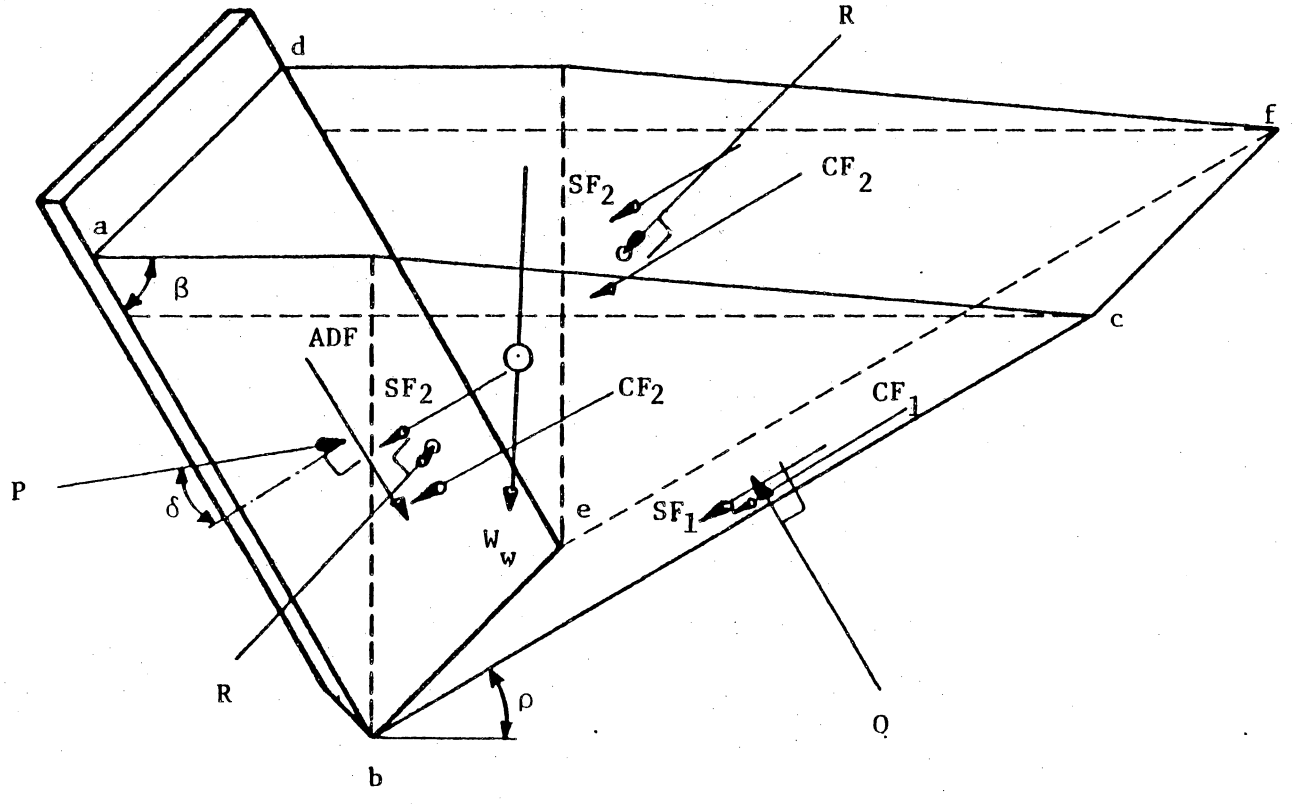

Figure 4 Idealized failure wedge with forces at failure (after Grisso, 1980).

where: R = force acting normal to surfaces abc and def, N

γ = unit weight of soil, N/cm^3

$K_o = 1-\sin(\phi)$

= coefficient of earth pressure at rest

$z = (D+H)/3$

= depth to centroid of the failure wedge, cm

A = area of each of the surfaces abc and def, cm^2

In terms of the dimensions in Figure 3:

$$A = (1/2)D^2(1+H/D)[(1+H/D)\cot(\beta)+\cot(\rho)] \quad \ldots\ldots\ldots\ldots\ldots\ldots(11)$$

where: D = tool depth, cm

H = height of soil heave in front of the tool, cm

β = angle the tool makes with the horizontal, cm

ρ = angle the rupture plane makes with the horizontal, degrees

Expressions for the other two forces acting on the side planes are:

$$SF_2 = R\tan(\phi) \quad \ldots\ldots\ldots\ldots\ldots\ldots\ldots\ldots\ldots\ldots\ldots\ldots\ldots\ldots\ldots\ldots(12)$$

$$CF_2 = cA \quad \ldots\ldots\ldots\ldots\ldots\ldots\ldots\ldots\ldots\ldots\ldots\ldots\ldots\ldots\ldots\ldots\ldots\ldots(13)$$

where: ϕ = angle of internal friction of the soil, degrees

c = soil cohesion factor, N/cm^2

SF_2 = the frictional force on the side planes, N

CF_2 = the cohesional force on the side planes, N

Three analogous force vectors (Q, CF_1, and SF_1) existed on the rupture surface bcfe (Figure 4). Vector Q is a normal force on the rupture surface and drops out of the final equation for the tool force. Expressions for the magnitudes of the other two force vectors are:

$$CF_1 = cBD/\sin(\rho) \qquad (14)$$

$$SF_1 = Q\tan(\phi) \qquad (15)$$

where: SF_1 = the frictional force on the rupture surface, N

CF_1 = the cohesional force on the rupture surface, N

Two forces acting on the soil-tool interface (face abed) include an adhesional force along the interface, resisting movement of the wedge on the tool, and the tool force (P) acting at an angle (δ) with the normal to the tool surface. This angle is the same as the soil-metal friction angle. The relationship for the adhesional force is:

$$ADF = A_d BD(1+H/D)/\sin(\beta) \qquad (16)$$

where: A_d = soil-metal adhesion factor, N/cm^2

The last force vector considered included the the weight of the soil wedge (W_w) and it is expressed as:

$$W_w = \gamma BA \qquad (17)$$

Summing the forces in the horizontal and vertical directions yielded the following equations:

$$P\sin(\beta+\delta) = -ADF\cos(\beta) + Q\sin(\rho) + (2SF_2+SF_1+2CF_2+CF_1)\cos(\rho) \quad \ldots\ldots\ldots\ldots\ldots (18)$$

$$P\cos(\beta+\delta) = W_w + ADF\sin(\beta) - Q\cos(\rho) + (2SF_2+SF_1+2CF_2+CF_1)\sin(\rho) \quad \ldots\ldots\ldots\ldots\ldots (19)$$

An equation for the total tool force (P) was then obtained by combining equations (18) and (19):

$$P = [-ADF\cos(\beta+\phi+\rho) + W_w\sin(\phi+\rho) + (2SF_2+2CF_2+CF_1)\cos(\phi)]/[\sin(\beta+\phi+\rho+\delta)] \quad \ldots\ldots\ldots (20)$$

Equation (20) contains two unknowns, the tool force (P) and the rupture angle (ρ). All terms on the right hand side of equation (20) could be computed if the rupture angle (ρ) and the height of soil heave (H) were known. During preliminary tests for development of the quasi-static model, very little soil accumulation was observed in front of the tool, and hence the variable (H) was assumed to be zero during the study. Since tool movement in the soil created a passive condition, Passive Earth Pressure Theory was used to determine the rutpure angle. According to Passive Earth Pressure Theory (Terzaghi, 1943), passive failure takes

place when the resistance by the soil wedge is minimum. The wedge which created the minimum resistance was found by minimizing the tool force (P) with respect to the rupture angle (ρ). Since differentiation of equation (20) was impractical, a numerical procedure was employed to minimize this function. Force predictions using the model showed good agreement with forces measured during soil bin tests with an artificial soil. The tests were conducted at very low tool speeds, using a hand-crank mechanism to move the tool (Grisso, 1980).

3.2.2 Model for predicting narrow tine behavior under dynamic conditions.

The major step involved in converting the quasi-static model to a dynamic model for narrow tines was to include terms which accounted for the accelerational force. A modification of the accelerational force equation developed by Soehne (1956) was used for this purpose. Since the accelerational force depended on the total mass of soil moved by the tool, a more accurate estimation of the size of the wedge was important, and hence the idealized soil wedge of Figure 3 could not be used for the dynamic model. Instead, a full failure wedge similar to the one in Figure 2 was utilized. The center and side sections of the wedge were considered seperately. For this analysis also, the rupture

surface was assumed to be a straight surface inclined at an angle, ρ, with the horizontal.

The force vectors acting on the center wedge are shown in Figure 5. The accelerational force F_{a1} is represented as a body force resisting acceleration of the wedge and is considered to act parallel to the rupture surface. An expression for the magnitude of this force is:

$$F_{a1} = (\gamma/g)BDV^2\sin(\beta)/\sin(\beta+\rho) \quad \text{.....(21)}$$

where: g = the gravitational constant, 980 cm/s^2

V = tool speed, cm/s

A uniform surcharge pressure, q, is assumed on the surface of the wedge. The load from the soil heaved in front of the tool (H used in the quasi-static model) could be considered as a part of this surcharge. An expression for the total force contributed by the surcharge pressure is:

$$F_{q1} = qBr \quad \text{.....(22)}$$

An expression for the rupture distance, r, is:

$$r = (1/2)D^2[\cot(\beta)+\cot(\rho)] \quad \text{.....(23)}$$

Three force vectors act on the soil rupture surface of the center wedge (surface bcfe in Figure 5). These force vectors are equivalent to those acting on the rupture surface

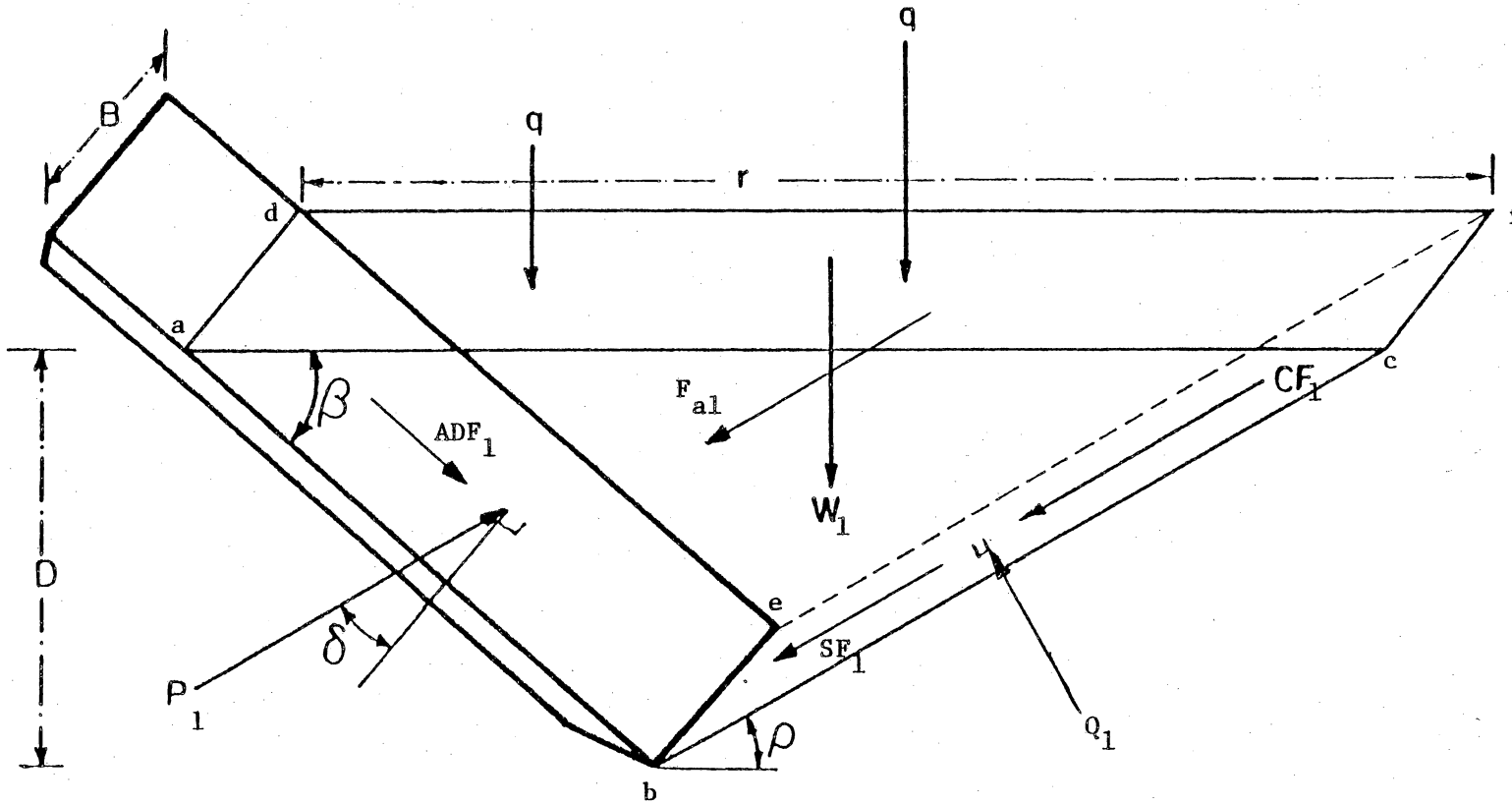

Figure 5 Center portion of the typical failure wedge considered for the dynamic model with forces at failure.

of the wedge considered in the quasi-static model. Vector Q_1 is the normal force on the surface and drops from the equations when solving for the tool force. Expressions for the magnitudes of the other two forces are:

$$CF_1 = cBD/\sin(\rho) \quad \text{.....(24)}$$

$$SF_1 = Q_1\tan(\phi) \quad \text{.....(25)}$$

The tool force due to the center portion of the failure wedge is designated as P_1 and acts at an angle δ to the normal to the tool surface. The relationship for the adhesional force ADF_1 resisting movement of the wedge on the tool is:

$$ADF_1 = A_dBD/\sin(\beta) \quad \text{.....(26)}$$

One remaining force vector is the weight weight vector, and it is expressed as:

$$W_1 = (1/2)\gamma BDr \quad \text{.....(27)}$$

Summing forces in the horizontal and vertical directions, the expressions for the horizontal and vertical forces respectively are:

$$P_1\sin(\beta+\delta) = -ADF\cos(\beta) + Q_1\sin(\rho) + (SF_1+CF_1+F_{a1})\cos(\rho) \quad \text{.....(28)}$$

$$P_1\cos(\beta+\delta) = W_1 + F_{q1} + ADF\sin(\beta) - Q_1\cos(\rho) + (SF_1+CF_1+F_{a1})\sin s(\rho) \quad \ldots\ldots\ldots\ldots\ldots\ldots(29)$$

Combining equations (28) and (29), P_1 can be expressed as:

$$P_1 = [-ADF\cos(\beta+\phi+\rho) + (W_1+F_{q1})\sin(\phi+\rho) + (CF_1+F_{a1})\cos(\phi)]/[\sin(\beta+\phi+\rho+\delta)] \quad \ldots\ldots\ldots(30)$$

The dynamic model also included terms to account for the tool force due to the side sections of the wedge (Figure 2). The center and side wedges were considered to move together as a bulb, and hence no tangential forces were considered on the planes between the two. A top view of the failure wedge is shown in Figure 6. At the soil surface the side wedges appeared to be two circular sectors of radius equal to the rupture distance, r.

The extreme outer points of the side wedges were initially assumed to lie in a vertical plane passing through the forward tip of the tool, as can be seen in Figure 2. This created the angle θ' at the soil surface (Figure 6). However, it was found that this caused overpredictions of the size of the side wedges and the total tool force. Based on this observation, a series of tests was conducted in the soil bin to determine the size of the failure wedge more accurately. To measure the soil disturbance, tines were

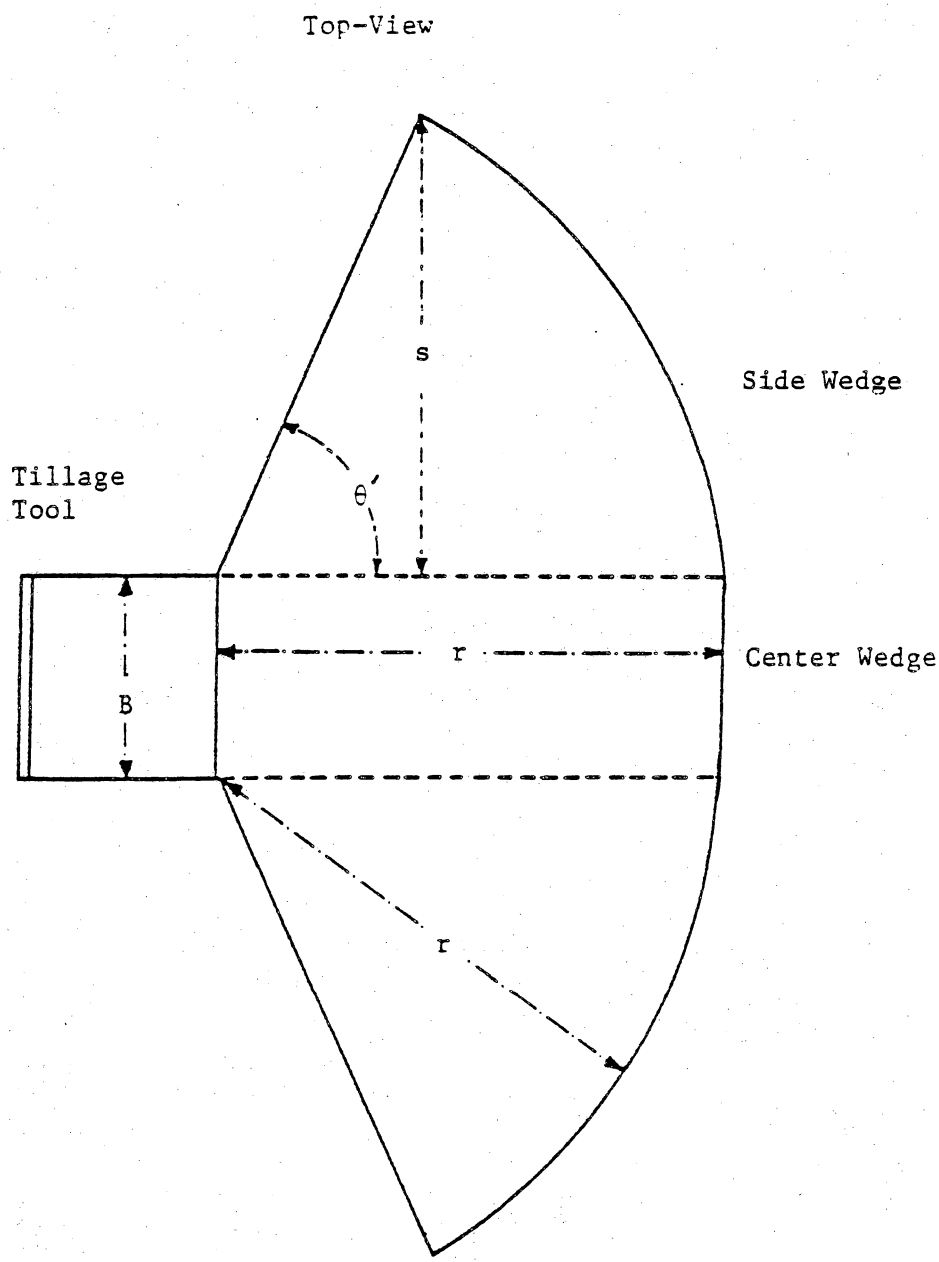

Figure 6 Top view of soil failure wedge considered for dynamic model.

pulled through the soil at extremely low speeds, until a failure wedge was fully formed. The general shape of the top of the failure wedge was similar to that in Figure 6. During each test, the rupture distance (r) and the maximum width of the side wedge (s) as illustrated in Figure 6 were measured. Tests were conducted for different combinations of tool width, angle, and depth. Soil conditions were kept constant. Experimental data thus collected is presented in Table A-1. Using this data and least squares regression, the following relation was developed which could be used to predict s if the tool angle and rupture distance were known:

$$s = -6.03 \text{ cm} + 0.460(r) + 0.0904(\beta) \quad \ldots\ldots\ldots\ldots\ldots\ldots (31)$$

where: s = maximum width of the side wedge, cm

β = tool angle, degrees

r = rupture distance, cm

The results presented in Figure 7 show high correlation between observations and prediction lines.

Equation (31) was used to modify the side wedges used initially. The side wedges as viewed from the top (Figure 6) were still assumed to be circular sectors of radius r, but the internal angle θ' was changed. Considering the geometry of the side wedges:

$$\theta' = \arcsin(s/r) \quad \ldots\ldots\ldots\ldots\ldots\ldots\ldots\ldots\ldots\ldots\ldots\ldots (32)$$

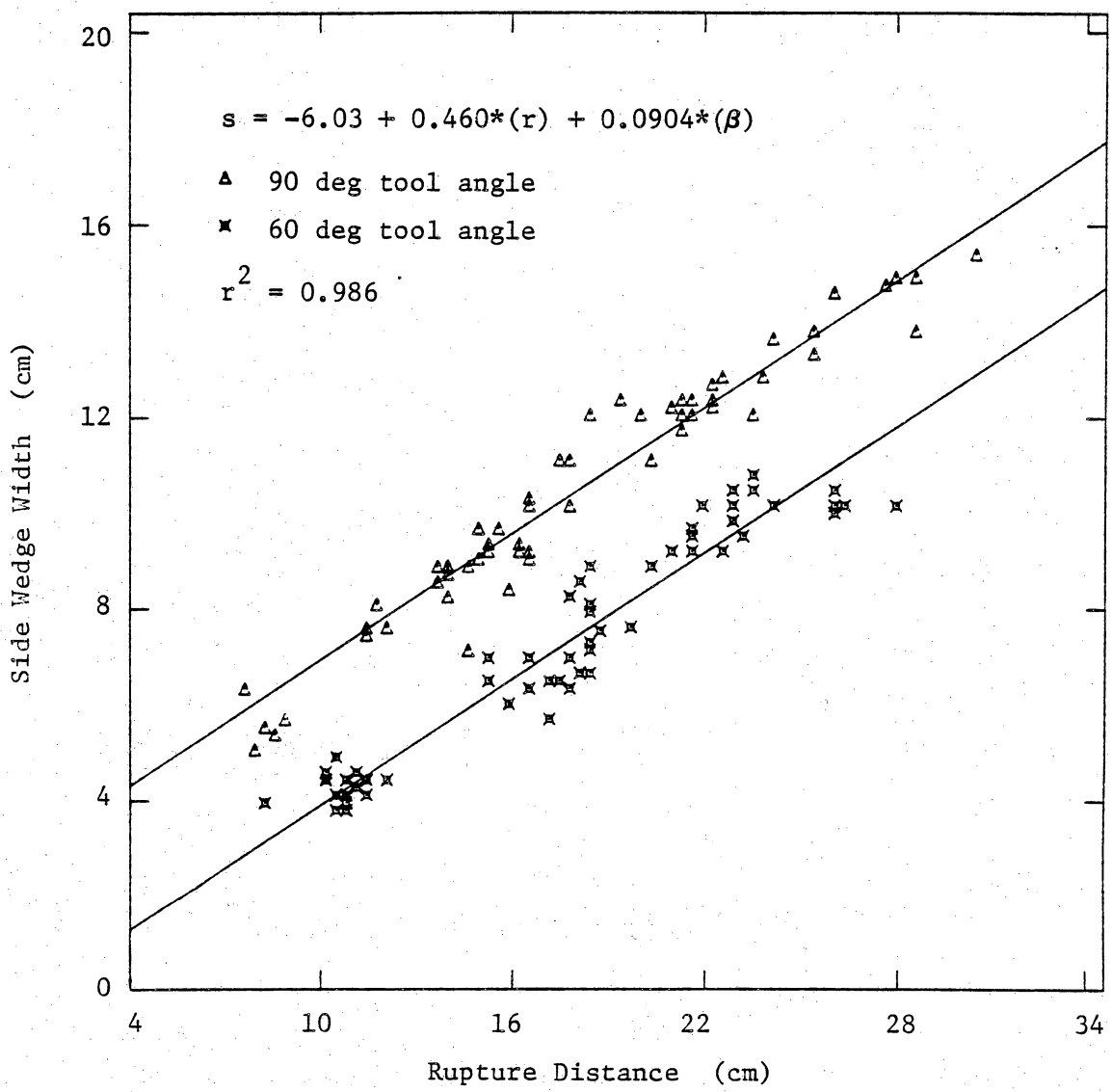

Figure 7 Side wedge width as a function of rupture distance and tool angle.

Using the regression relationship of equation (31):

$$\theta' = \arcsin\{[-6.03 + 0.460(r) + 0.0904(\beta)]/r\} \quad \ldots\ldots\ldots(33)$$

To determine the component of the tool force contributed by one of the side wedges, a differential element of angle $d(\theta)$, shown in Figure 8 with the force vectors acting on it, was considered. Since the side wedges had no contact with the tool face, there were no adhesional forces. The accelerational force, F_{a2}, contributed by the differential element acted parallel to the rupture surface, resisting movement of the wedge. An expression for the differential accelerational force is:

$$dF_{a2} = f_{a2}d\theta \quad \ldots\ldots\ldots(34)$$

where:

$$f_{a2} = (1/2)(\gamma/g)DrV^2\sin(\beta)/\sin(\beta+\rho) \quad \ldots\ldots\ldots(35)$$

An expression for the differential force contributed by the surcharge pressure is:

$$dF_{q2} = f_{q2}d\theta \quad \ldots\ldots\ldots(36)$$

where:

$$f_{q2} = (1/2)qr^2 \quad \ldots\ldots\ldots(37)$$

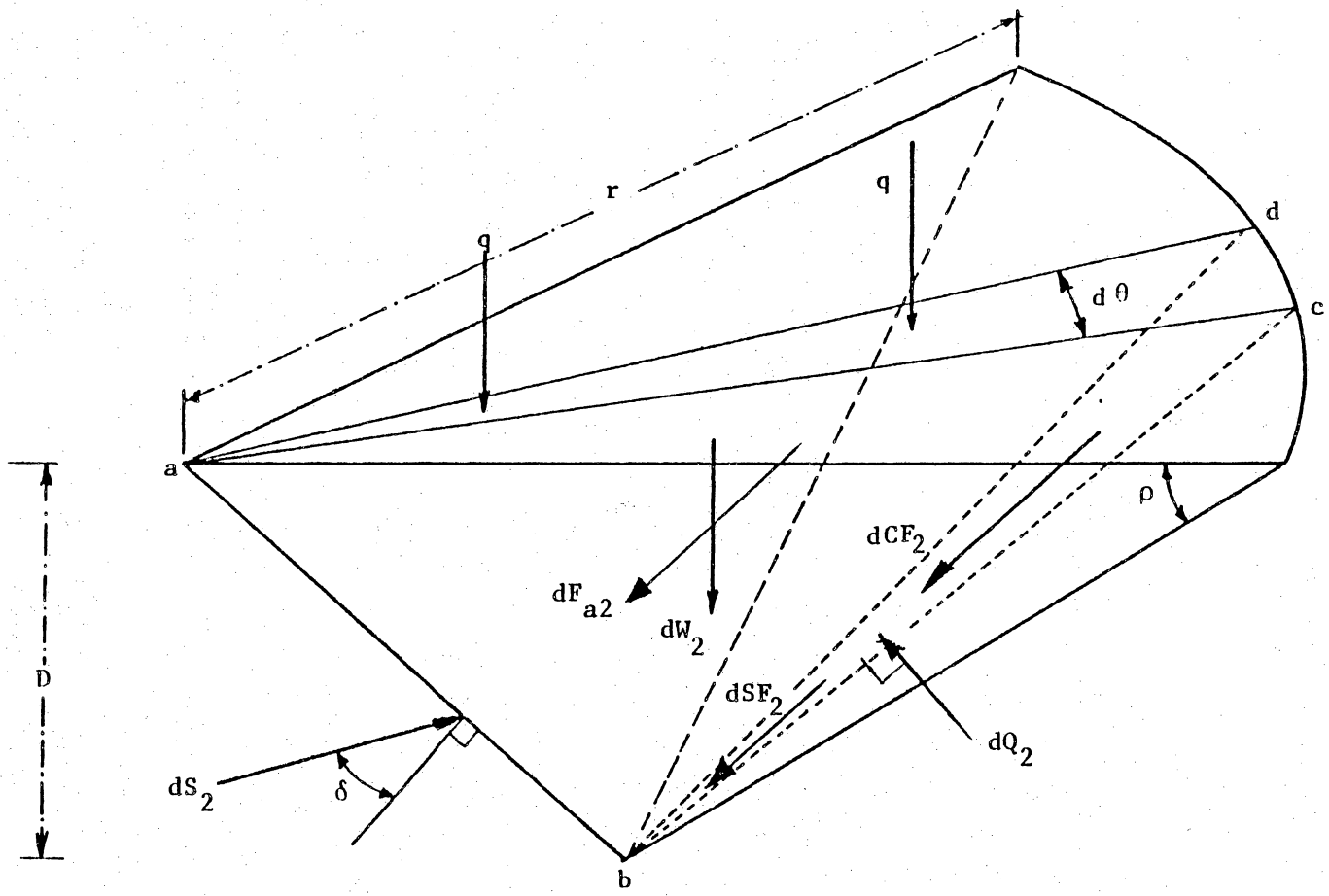

Figure 8 A side portion of the typical failure wedge considered for the dynamic model with forces at failure.

Three forces (dCF_2, dSF_2, dQ_2) acting on the rupture surface (face bcd) are analogous to those on the center wedge. The normal force dQ_2 is eliminated from the equations when solving for the tool force. Expressions for the other two forces are:

$$dSF_2 = dQ_2 \tan(\phi) \quad \text{.....(38)}$$

$$dCF_2 = cf_2 d\theta \quad \text{.....(39)}$$

where:

$$cf_2 = (1/2)cDr/\sin(\rho) \quad \text{.....(40)}$$

An expression for the weight of the differential element is:

$$dW_2 = w_2 d\theta \quad \text{.....(41)}$$

where:

$$w_2 = (1/6)\gamma Dr^2 \quad \text{.....(42)}$$

The incremental force dS_2 acts at the same angle with the horizontal as did the center wedge force P_1. Summing the forces in the horizontal and vertical directions, the relationships for the horizontal and vertical forces resulting from each differential element can be written as:

$$dS_2 \sin(\beta+\delta) = dQ_2 \sin(\rho) + (dSF_2 + dCF_2 + dF_{a2}) \cos(\rho) \quad \text{.....(43)}$$

$$dS_2\cos(\beta+\delta) = dW_2 + dF_q - dQ_2\cos(\rho) + (dSF_2+dCF_2+dF_{a2})\cos(\rho) \quad \ldots\ldots(44)$$

Combining equations (43) and (44):

$$dS_2 = [(dW_2+dF_{q2})\sin(\phi+\rho)d\theta + (dCF_2+dF_{a2})\cos(\phi)]/[\sin(\beta+\phi+\rho+\delta)] \quad \ldots\ldots(45)$$

The incremental force dS_2 acts in a vertical plane that makes an angle θ with the path of the tool. The component of the incremental force acting in a vertical plane containing the path of tool is thus:

$$dP_2 = dS_2\cos(\theta) \quad \ldots\ldots(46)$$

Due to the symmetry of the failure geometry, the forces from the two side wedges acting perpendicular to the direction of travel cancelled each other.

For one side wedge, the total tool force in the direction of movement was then:

$$P_2 = \int_o^{\theta'} dP_2 d\theta \quad \ldots\ldots(47)$$

After integrating:

$$P_2 = [(w_2+f_{q2})\sin(\phi+\rho)\sin(\theta') + fa_2\cos(\phi)(\theta'/2 + \sin(2\theta')/4) + (cf_2\cos(\phi)\sin(\theta')]/[\sin(\beta+\phi+\rho+\delta)] \quad \ldots\ldots(48)$$

The total tool force with contributions from the center wedge and the two side wedges was expressed as:

$$P = P_1 + 2P_2 \quad \text{.....(49)}$$

Equation (49) contains two unknowns, the total force P and the rupture angle ρ, as did equation (20). As in the quasi-static model, a numerical procedure was used to minimize P and to identify a wedge of least resistance. The draft force, lift force, and the normal force acting on the tool could then be determined from the total force. The expressions for each are as follows:

$$P_x = P\sin(\beta+\delta) \quad \text{.....(50)}$$

$$P_z = -P\cos(\beta+\delta) \quad \text{.....(51)}$$

$$P_n = P_x/[\sin(\beta)+\cos(\beta)\tan(\delta)] \quad \text{.....(52)}$$

where: P_x = the predicted draft force

P_y = the predicted lift force

P_n = the predicted force normal to the tool face

3.3 LABORATORY TESTS FOR MODEL VERIFICATION.

Experimental verification tests were conducted under controlled conditions using an indoor soil bin facility (Durant, 1979; Durant et al., 1980). This section provides a brief description of the soil bin facility, soil type used, and the procedure employed for the verification tests.

3.3.1 Soil bin facility.

The soil bin facility at Virginia Polytechnic Institute and State University (Figure 9) is comprised of the following functional components: a soil bin, soil processing carriage, tool carriage, drive system, controls and data acquisition system. The bin, which holds the test section, is approximately 10 m long, 0.9 m wide, and 0.4 m deep. Solid steel beams on each side of the bin support the soil processing and tool carriages.

The soil processing carriage is used to prepare the test section before each test. It includes a conventional tiller assembly powered by an electric motor for loosening and mixing the soil, an adjustable strike off blade for leveling the soil surface, and a teflon coated roller for compacting the soil. The entire assembly, the soil processing unit, is supported by four sets of wheels and can move back and forth on the steel beams when pulled by the tool carriage.

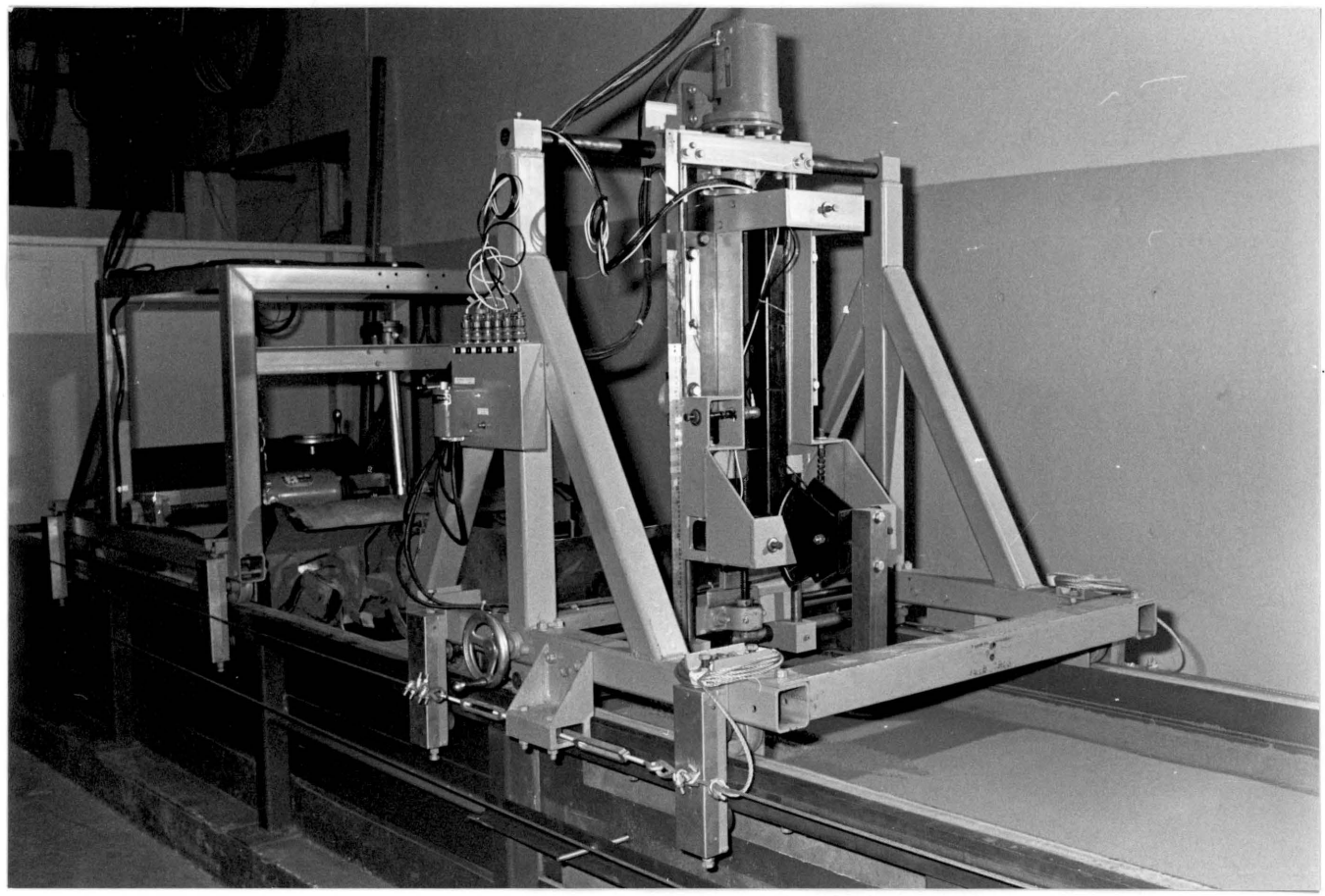

Figure 9 An overall view of the soil bin facility used in verification tests.

The tool carriage supports a dynamometer with six load cells positioned to sense forces in the x, y, and z directions as well as moments about the three axes (Figure 10). A tool plate with provisions to vary the tool angle is attached to the dynamometer. The tool carriage is supported by four sets of wheels and is connected to the drive system. A solenoid-activated latch system is provided on the tool carriage to pull the soil processing unit when needed.

The drive system consists of an electronically controlled hydrostatic transmission driven by an electric motor. This in turn drives a cable and sheave system to move the tool carriage.

The controls include a main control panel for activating the various soil bin components and a servo control panel for controlling the speed and acceleration and deceleration of the tool carriage.

The data acquisition system (Cline and Perumpral, 1982) utilizes an ADAC Corporation 1000 system with the capability to digitize low-level analog signals, such as those produced by strain gages, from 16 channels. Also, it can perform precise time measurements and detect 16 switch contact closures. The system provides exicitation to the dynamometer load cells and performs operations on the output signals.

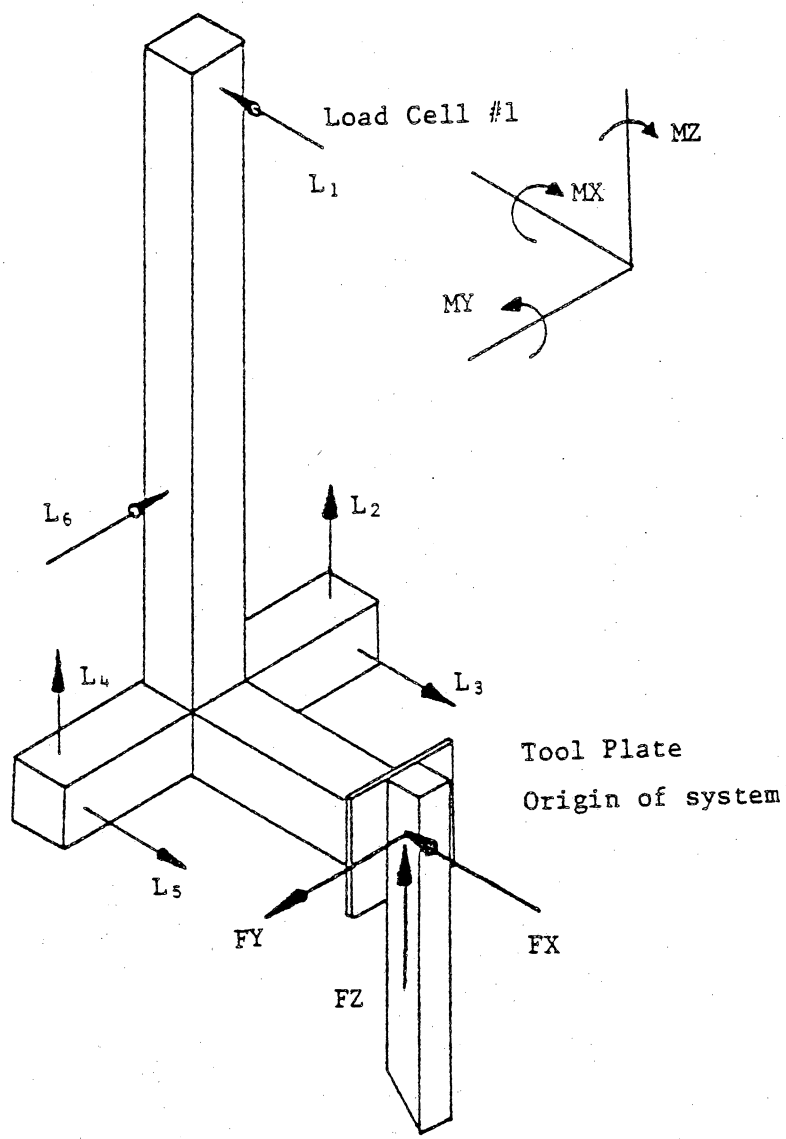

Figure 10 Load cell locations on the dynamometer used for recording tool forces and moments.

3.3.2 Soil description.

An artificial soil was used for tests. It consisted of equal weights of Florida Zircon sand and 50-mesh fire clay. This was mixed with 10 percent by weight of SAE 5 weight mineral oil to simulate moisture content. The artificial soil was used to minimize variations within the test section between tests.

3.3.3 Verification tests.

Prior to each test, the soil was tilled and the surface was leveled. The soil was compacted with four passes of the compaction roller. This resulted in an average soil density of 1.87 g/cc over the upper 20 cm of soil.

The tools used in the tests were flat tines constructed from cold-rolled steel stock 13 mm thick. The edges of the tools were beveled to avoid friction on the tool sides. The tool of desired width was mounted on the tool plate, and the depth and tool angle were then set.

Desired tool speed and acceleration and deceleration rates were set on the control panel. The test was then conducted by pulling the tool through the soil at a predetermined speed. The first 1.5 m travel distance was utilized to allow the tool carriage to reach a steady speed, and hence no data was recorded. Transducer outputs were record-

ed during the next 1 m of tool travel. Microswitches located at either end of the 1 m test section activated and deactivated the data acquisition system. The sample rate varied from one reading every 0.034 s for the fastest tool speed, to one every 0.30 s for the slowest tool speed. Each set of transducer signals was then converted to force and moment readings using a matrix procedure (Perumpral et al., 1980) and displayed or stored. After completing the tests, values of the forces in each direction and the moments about each axis were averaged over each test.

Due to the symmetry of the tools, the forces in the y direction and the moments about the x and z axes (Figure 10) were approximately zero, and hence were not considered for further analysis. The forces in the x and z directions were investigated and used for model verification.

The forces in the x and z directions along with the moment about the y axis were used to locate the depth at which the total resultant tool force occurred. The major assumption in calculating this depth was that the soil could not impose a moment on the tool other than that created by the total force. According to Passive Earth Pressure Theory (Terzaghi, 1943) the resultant would be at a depth between one-half and two-thirds of the tool depth.

Also for model verification, the values of the forward rupture distance (r) and the width of the side wedge (s) predicted by the model were compared to the measured values. The measurements of r and s were taken during the series of tests described previously in the model development section for investigating the size and shape of the total failure wedge. These measurements were averaged over each combination of tool angle, tool depth, and tool width for comparison with the predicted values.

3.3.4 Variables considered during verification tests.

The soil bin tests for model verification were conducted using four tool widths, three tool depths, three tool angles, and four tool speeds. This resulted in 144 possible combinations of these four independent variables. A subset of 27 combinations was chosen for testing, with two tests conducted for each combination. This subset was systematically chosen using a partial replication scheme designed for analysis of variance procedures (Cochran and Cox, 1957). The theory behind the scheme is to use a minimal number of mutually orthogonal contrasts to adequately cover the four-dimensional space of these independent variables. All parameters other than width, depth, angle, and speed remained constant, and the values used for each variable are as follows:

Tool width (B) 2.5, 5.1, 7.6, and 10.2 cm

Tool depth (D) 5.1, 10.2, and 15.2 cm

Tool angle (β) 60, 75, and 90 degrees

Tool speed (V) 5.4, 33.1, 67.1, and 120. cm/sec

Surcharge (q) assumed zero

Soil cohesion factor (c) 0.219 N/cm^2

Soil internal friction angle (ϕ) 36.3 degrees

Soil weight density (γ) 0.0182 N/cm^3 (1.86 g/cc)

Soil-metal adhesion factor (A_d) 0.193 N/cm^2

Soil-metal friction angle (δ) 50.5 degrees - 0.45(β)

The soil strength parameters c and ϕ and the soil-metal adhesion factor A_d were those obtained from the direct shear and friction tests described earlier. The soil-metal friction angle (δ) values were based on the relationship developed by Grisso (1980).

Chapter IV

RESULTS AND DISCUSSION

4.1 SOIL SHEAR STRENGTH AND SOIL-METAL FRICTION.

4.1.1 Shear rate effect on soil shear strength.

The results of the soil shear strength tests are presented in Figure 11, by plotting shear stress vs. normal stress for all shear rate considered. The raw experimental data is given in Table A-2. Least squares regression equations were fitted to the data for each shear rate and the coefficients of determination for these regressions are 0.990 or higher. The high coefficient of determination values indicate that the assumption that the soil fails according to the Mohr-Coulomb criterion is valid. The angle of internal friction (ϕ) and the cohesion factor (c) were obtained from the slope and the vertical axis intercept of the regression lines respectively. Pairwise tests of equality were conducted on the slopes and on the intercepts of the regression equations (Koopmans, 1981). No significant differences were found between any of the slopes or intercepts at the 5 % level.

The observation that the strength parameters are independent of shear rate contradicts observations from previous studies. Rowe and Barnes (1961) and Stafford and Tanner (1983a) found that shear strength increased with increasing

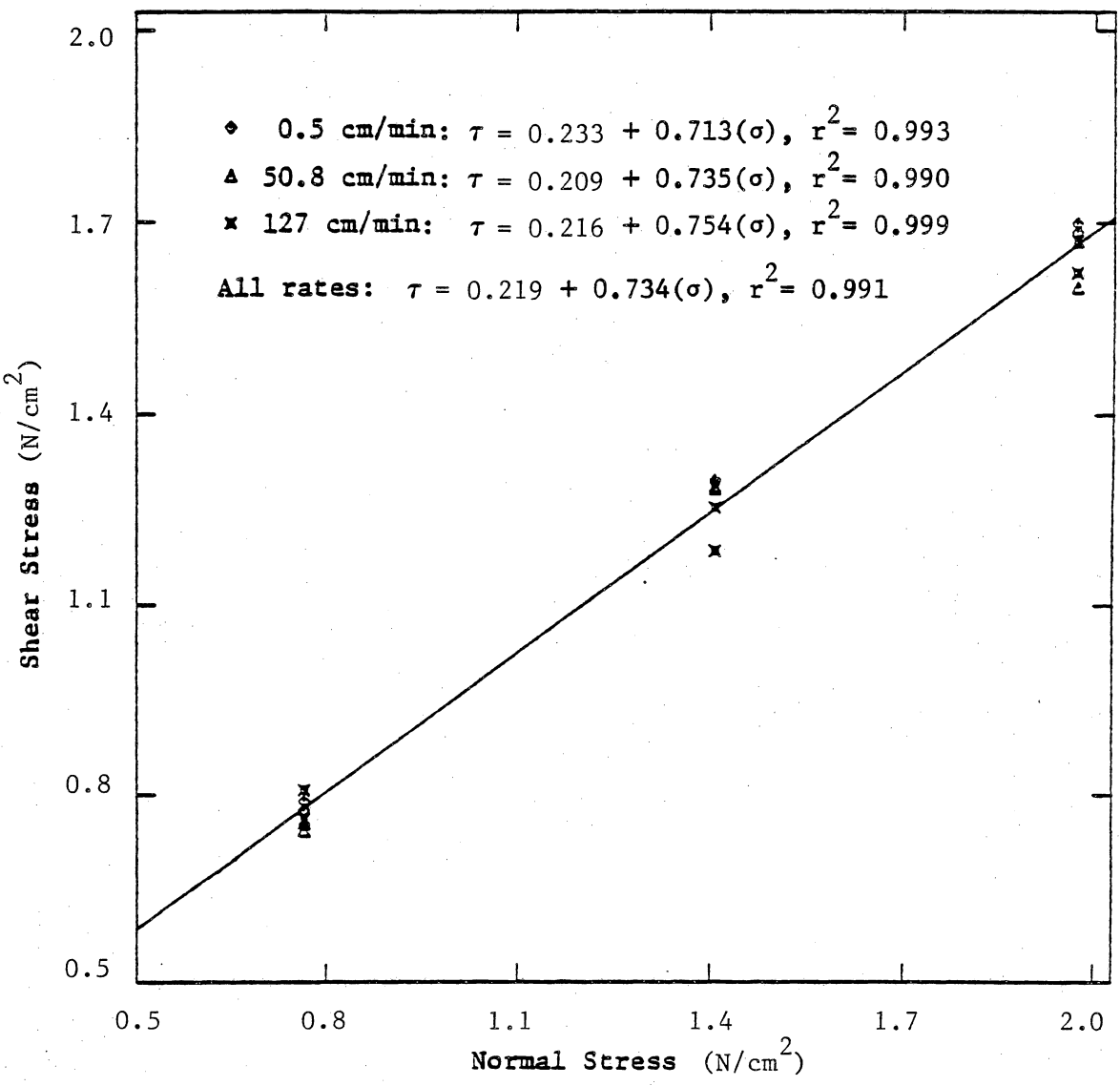

Figure 11 Shear stress vs. normal stress relationship from direct shear tests on artificial soil.

shear rate. Both studies used torsional shearing devices. Results of tests conducted by Stafford and Tanner at different normal stress and shear rates showed an increase in cohesion as a function of shear rate, but showed that the angle of internal friction to be independent of shear rate. The shear rates used in the present study were comparatively lower. However, Stafford and Tanner found maximum influence at low shear rates.

The reason for this disagreement between results is not known fully. The procedure used for shear tests in this study appears to be valid. As can be observed in Figure 11, the results were quite repeatable. The coefficients of determination for the linear regression equations are very high. Also, the c and ϕ values obtained agree well with those obtained from triaxial tests (Sture et al., 1980).

To determine whether or not the disagreement was caused by the mineral oil present in the artificial soil, direct shear tests were conducted on samples of the dry artificial soil. As would be expected, the cohesion was lower for the dry soil, and the internal friction angle was basically unchanged. Additional statistical analysis conducted on the dry soil showed that the shear rate had no effect on the soil strength parameters.

Considering the results of all direct shear tests conducted during this study, it appears that the discrepancy in shear rate effect on shear strength may be the result of the difference in test procedures between torsional and direct shear tests. Further investigation into this discrepancy is needed, with the same soil being tested using both procedures.

Since the strength parameters for the artificial soil were found to be independent of shear rate for the ranges tested, the results presented in Figure 11 were pooled to obtain the c and ϕ values. The regression equation for the same is given in Figure 11, and the c and ϕ values are 0.219 N/cm^2 and 36.3 degrees respectively.

4.1.2 Shear rate effect on soil-metal friction.

The results of the soil-metal friction tests are presented in Figure 12. The raw data is presented in Table A-3. Regression equations of shear stress vs. normal stress were fitted to the data for each shear rate, with the lowest coefficient of determination being 0.997. Pairwise comparisons on the slopes and on the intercepts showed no significant differences at the 5 % level, indicating that the soil-metal adhesion factor and soil-metal friction angle are independent of shear rate for the soil-metal combination consid-

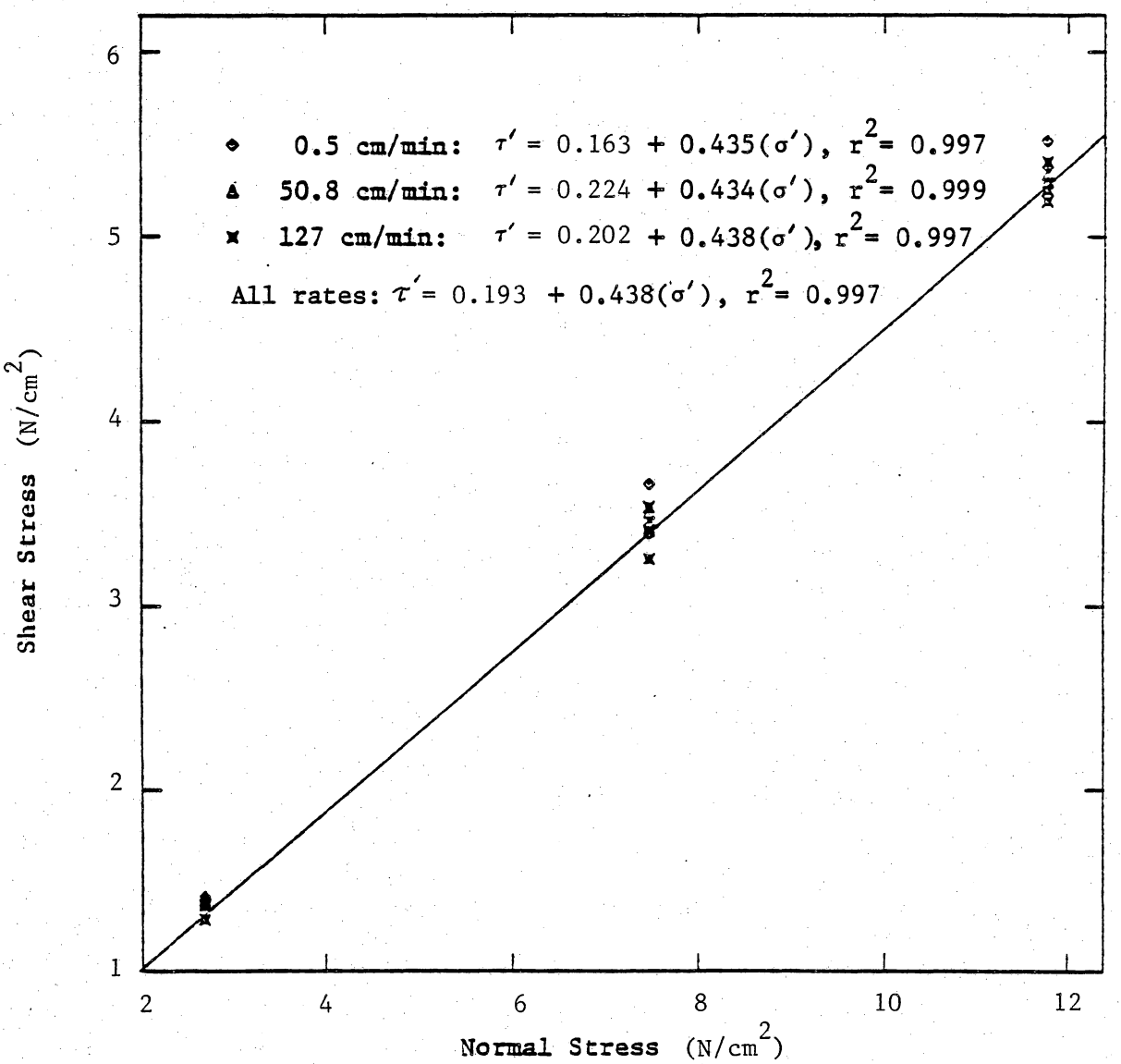

Figure 12 Shear stress vs. normal stress relationship from soil-metal friction tests with the artificial soil.

ered. Therefore, pooling the data from all tests, the values of A_d and δ were found to be 0.193 N/cm^2 and 23.6 degrees respectively. The regression equation in terms of A_d and δ is given in Figure 12.

The observation that A_d and δ are independent of shear rate contradicts the results of tests by Stafford and Tanner (1983b). Tests conducted using a torsional device at different normal stress and shear rates showed soil-metal friction angle to vary as a function of shear rate. No relation was found between adhesion and shear rate. Again, this discrepancy is believed to be a result of the difference in the procedures used.

4.2 LABORATORY TESTS FOR MODEL VERIFICATION.

Results of the 54 soil bin tests conducted are summarized in Table 1. For each test, the average values of draft force (FX), lift force (FZ), and moment about the tranverse axis (MY) are included. Also presented in the same Table are the predicted values of the two forces using the dynamic soil-tool interaction model developed during this study.

Table 1. Predicted and experimentally observed forces and moments from 54 soil bin tests.

Test Condition				Observed Values			Predicted Values	
B	β	D	V	FX	FZ	MY	PX	PZ
(cm)	(deg)	(cm)	(cm/s)	(N)	(N)	(N-m)	(N)	(N)
2.5	60	5.1	5.7	36.7	-2.5	-11.0	33.7	-3.8
2.5	60	5.1	5.7	37.2	-3.2	-11.1	33.7	-3.8
2.5	60	10.2	126.8	192.3	-34.7	-42.2	176.7	-20.1
2.5	60	10.2	127.2	185.0	-33.5	-41.3	176.9	-20.2
2.5	60	15.2	68.8	340.1	-56.7	-73.8	320.4	-36.5
2.5	60	15.2	68.7	371.3	-63.6	-81.1	320.3	-36.5
2.5	75	5.1	33.3	66.2	7.4	-18.5	52.9	1.6
2.5	75	5.1	33.3	66.4	7.5	-20.5	52.9	1.6
2.5	75	10.2	5.4	139.7	8.7	-40.8	172.5	5.3
2.5	75	10.2	5.3	116.9	9.9	-35.2	172.5	5.3
2.5	75	15.2	121.3	471.0	-11.4	-112.1	534.1	16.3
2.5	75	15.2	121.0	462.1	-10.2	-112.3	533.3	16.3
2.5	90	5.1	122.6	150.5	32.1	-47.2	116.3	20.5
2.5	90	5.1	122.4	152.3	30.6	-46.6	116.2	20.5
2.5	90	10.2	68.8	263.5	37.8	-78.9	295.8	52.2
2.5	90	10.2	68.8	271.9	36.6	-80.0	295.9	52.2
2.5	90	15.2	5.4	417.6	36.5	-123.9	558.9	98.5
2.5	90	15.2	5.4	466.2	39.0	-134.9	558.8	98.5
5.1	60	5.1	68.9	92.9	-9.4	-22.0	55.2	-6.3
5.1	60	5.1	68.8	93.0	-15.3	-20.9	55.2	-6.3
5.1	60	15.2	125.3	614.4	-74.4	-118.9	479.1	-54.6
5.1	60	15.2	125.4	573.2	-73.8	-111.1	479.3	-54.6
5.1	75	5.1	122.4	147.4	11.2	-37.5	99.8	3.1
5.1	75	5.1	122.3	153.2	12.0	-38.7	99.8	3.0
5.1	90	5.1	5.4	118.3	39.9	-40.6	107.8	19.0
5.1	90	5.1	5.4	101.9	33.6	-34.7	107.8	19.0
5.1	90	10.2	121.6	500.3	90.8	-141.6	447.4	78.9
5.1	90	10.2	121.2	470.1	89.1	-134.2	446.9	78.8

Table 1. (continued)

Test Condition				Observed Values			Predicted Values	
B	β	D	V	FX	FZ	MY	PX	PZ
(cm)	deg.	(cm)	(cm/s)	(N)	(N)	(N-m)	(N)	(N)
7.6	60	10.2	5.6	235.5	-26.4	-56.6	197.7	-22.5
7.6	60	10.2	5.6	230.9	-32.1	-55.3	197.7	-22.5
7.6	75	10.2	68.8	380.5	14.2	-95.7	297.9	9.1
7.6	75	10.2	68.8	410.4	18.4	-102.2	297.9	9.1
7.6	75	15.2	5.3	634.0	38.3	-154.4	544.9	16.7
7.6	75	15.2	5.3	619.5	31.3	-150.9	544.9	16.7
7.6	90	15.2	33.2	933.0	181.9	-247.3	790.5	139.4
7.6	90	15.2	33.1	839.9	159.2	-230.9	790.4	139.4
10.2	60	5.1	125.9	434.8	-102.3	-91.4	108.5	-12.4
10.2	60	5.1	126.2	389.6	-92.6	-79.9	108.7	-12.4
10.2	60	10.2	33.3	294.4	-63.1	-67.8	239.2	-27.2
10.2	60	10.2	33.3	292.7	-58.9	-68.3	239.2	-27.3
10.2	60	15.2	5.3	496.3	-94.0	-107.6	479.8	-54.7
10.2	60	15.2	5.2	544.2	-101.5	-115.4	479.8	-54.7
10.2	75	5.1	5.3	139.4	17.6	-40.3	109.6	3.3
10.2	75	5.1	5.3	128.0	17.5	-38.0	109.6	3.3
10.2	75	10.2	120.2	691.4	26.5	-168.1	418.6	12.8
10.2	75	10.2	121.0	572.5	20.2	-138.6	419.9	12.8
10.2	75	15.2	68.5	921.7	36.3	-209.9	690.0	21.1
10.2	75	15.2	68.4	885.7	39.5	-199.4	689.8	21.1
10.2	90	5.1	33.4	539.8	116.6	-156.1	163.6	28.8
10.2	90	5.1	33.3	578.5	125.1	-166.8	163.5	28.8
10.2	90	10.2	5.5	533.0	115.4	-142.9	443.2	78.2
10.2	90	10.2	5.4	499.2	113.8	-146.7	443.2	78.2
10.2	90	15.2	118.0	1242.2	246.4	-306.6	1150.5	202.9
10.2	90	15.2	117.8	1235.5	240.1	-305.1	1149.8	202.8

4.2.1 Draft force comparison.

The predicted and experimentally observed draft forces are presented in Figure 13 for comparison. If the magnitudes of both were equal, all points would lie on a line with a slope of one, passing through the origin. In general, the predicted values tend to be lower than the observed with an average prediction error (difference between predicted and experimental values) of -66.8 N. The least squares regression shown in Figure 13 indicates that the vertical intercept of the fitted line is very close to zero, but the slope is significantly different from one.

Figure 13 also shows that for a few cases the model overpredicts the draft force while for a few other cases it greatly underpredicts the draft. In an attempt to determine the reason for the discrepancies, the prediction error was plotted against the independent variables and combinations of the variables. One such plot (Figure 14) of prediction error and the ratio between tool depth and tool width (D/B) shows the underpredictions and overpredictions are maximum at low and high depth-width ratios respectively. At intermediate depth-width ratios, the predictions agree better with the experimental observations. The correlation coefficent between the prediction error and the depth-width ratio is 0.57 , and it is significantly different from zero at the

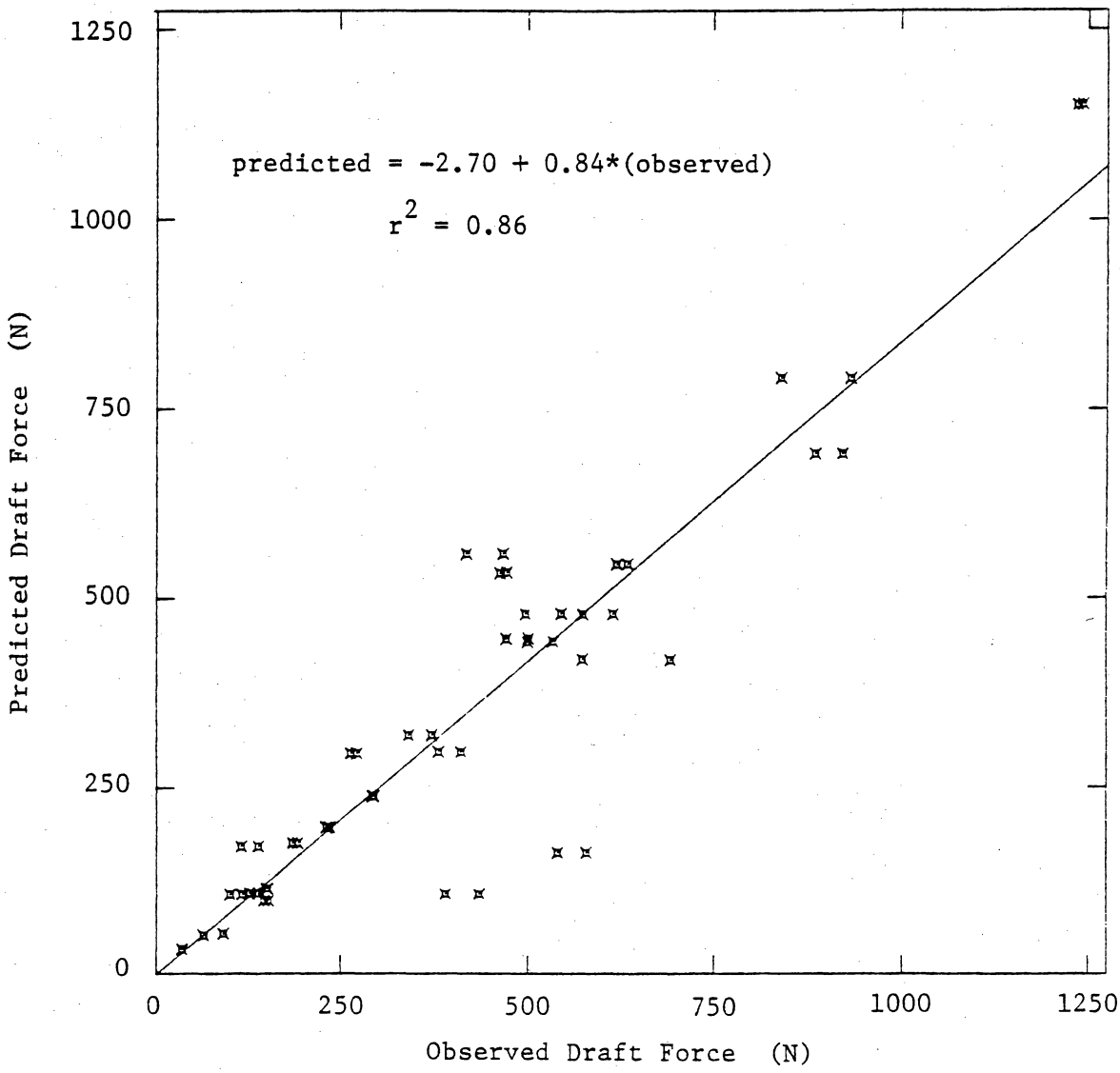

Figure 13 Comparison of predicted and experimentally observed draft force.

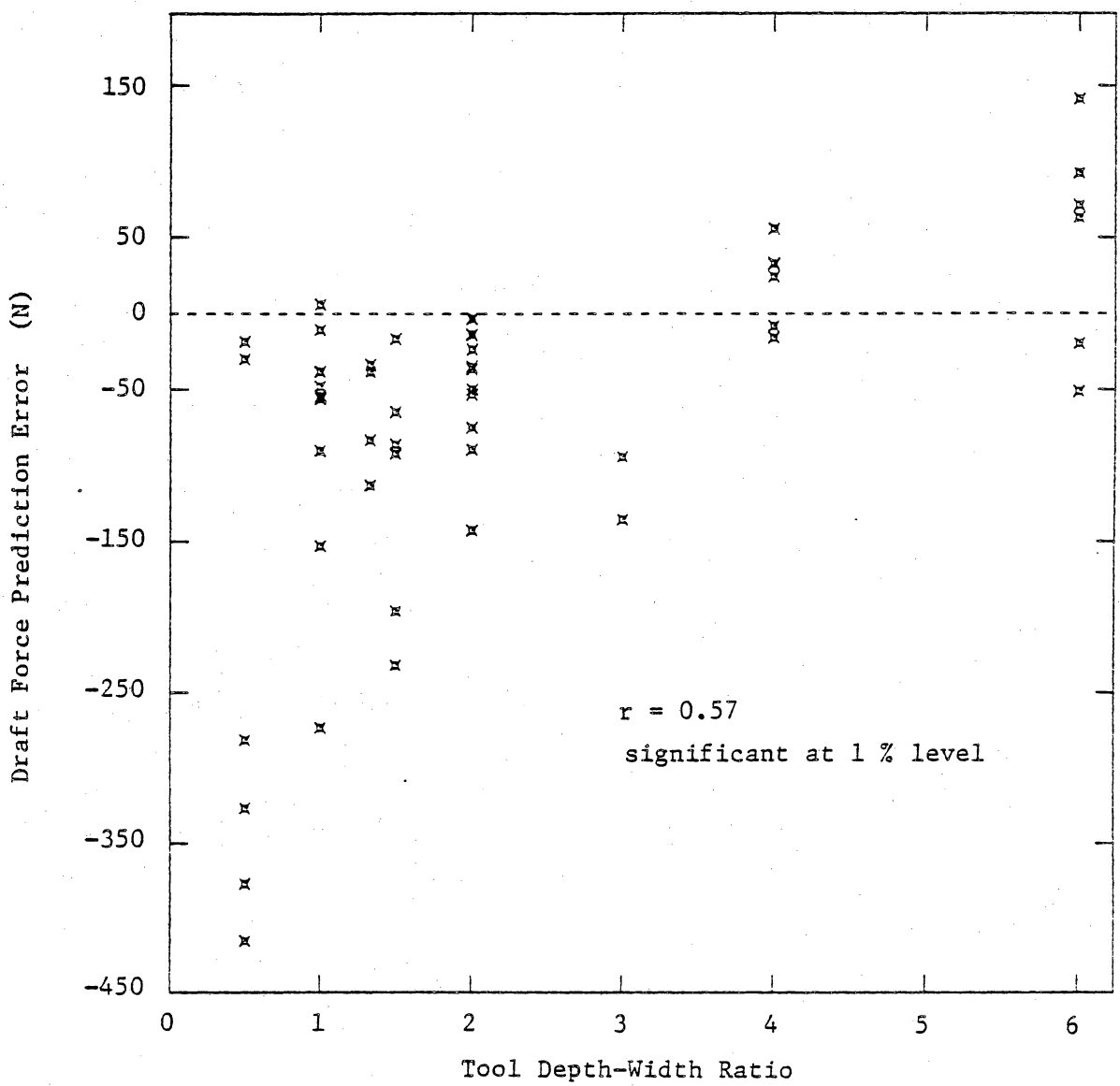

Figure 14 Effect of tool depth-width ratio on draft force prediction error.

1 % level. This shows a strong linear relationship between the two. The large underpredictions and overpredictions in the draft appear to be due at least partially to underpredictions and overpredictions of the size of the failure wedge. This is discussed more fully in Section 4.2.3.

A plot of the draft force prediction error vs. tool speed is shown in Figure 15. A definite relation between the error and tool speed is not observed. The correlation coefficient between the two is -0.22, and it is not significantly different from zero. In the soil-tool interaction model, the terms containing tool speed are the accelerational force terms. Due to the fact that a large increase in draft force is observed to occur over the speed range used, while the prediction error does not vary as a function of tool speed, it appears that the accelerational force terms used in the model do account for a large portion of increase in tool force as originally hypothesized.

This observation contradicts the findings of others (Rowe and Barnes, 1961; Siemens et al., 1965; Wismer and Luth, 1972) who used Soehne's (1956) equation to predict accelerational forces. It is believed, however, that these investigators used the equation alone to predict the accelerational force component, and then added the component to their static predictions. In this model, the accelerational forces

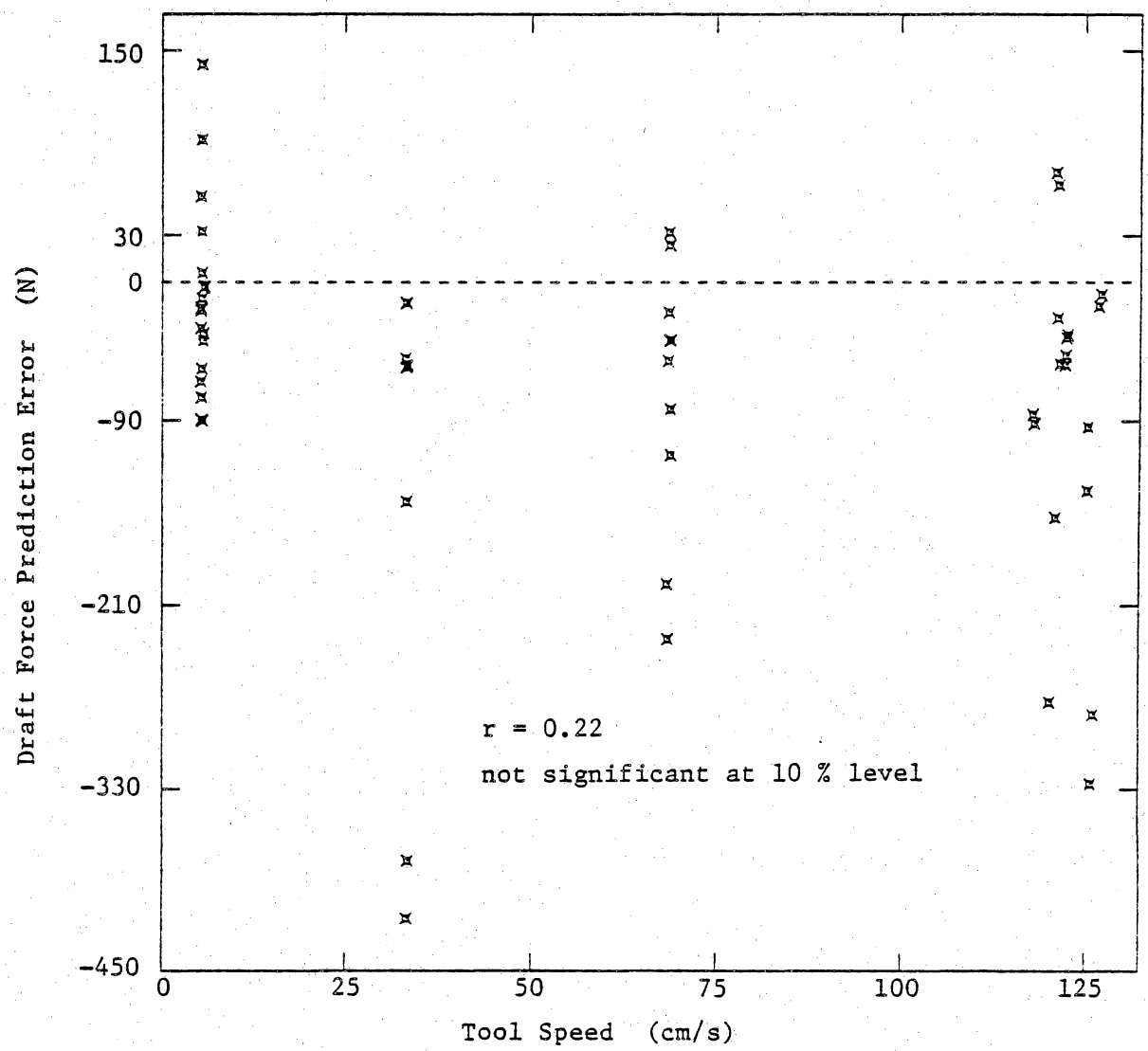

Figure 15 Effect of tool speed on draft force prediction error.

were included when summing all forces on the failure wedge. Summing the forces in Figures 5 and 8 (including the accelerational forces) and setting the sums equal to zero, is equivalent to summing all forces other than the accelerational forces and equating these to the product of mass and acceleration of the wedge as stated by Newton's Second Law of motion. The result is that the terms included in Soehne's equation are modified by including variables describing the failure geometry (internal angle of friction, soil-metal frictional angle, tool angle, and rupture angle) as shown in equations (20) and (48).

It should also be noted that for tillage tools, the magnitude of the draft force is generally much larger than the lift force. This was the case for the soil bin tests also, and hence the total tool force relationships were very similar to those of the draft force. Thus, the above discussion on the draft force applies to the total tool force also.

4.2.2 Lift force comparison.

A plot of predicted and experimentally observed values of lift force is presented in Figure 16. The agreement between the two is comparatively poor. In the least squares regression equation for the relationship (Figure 16), the intercept and slope are significantly different from zero and one

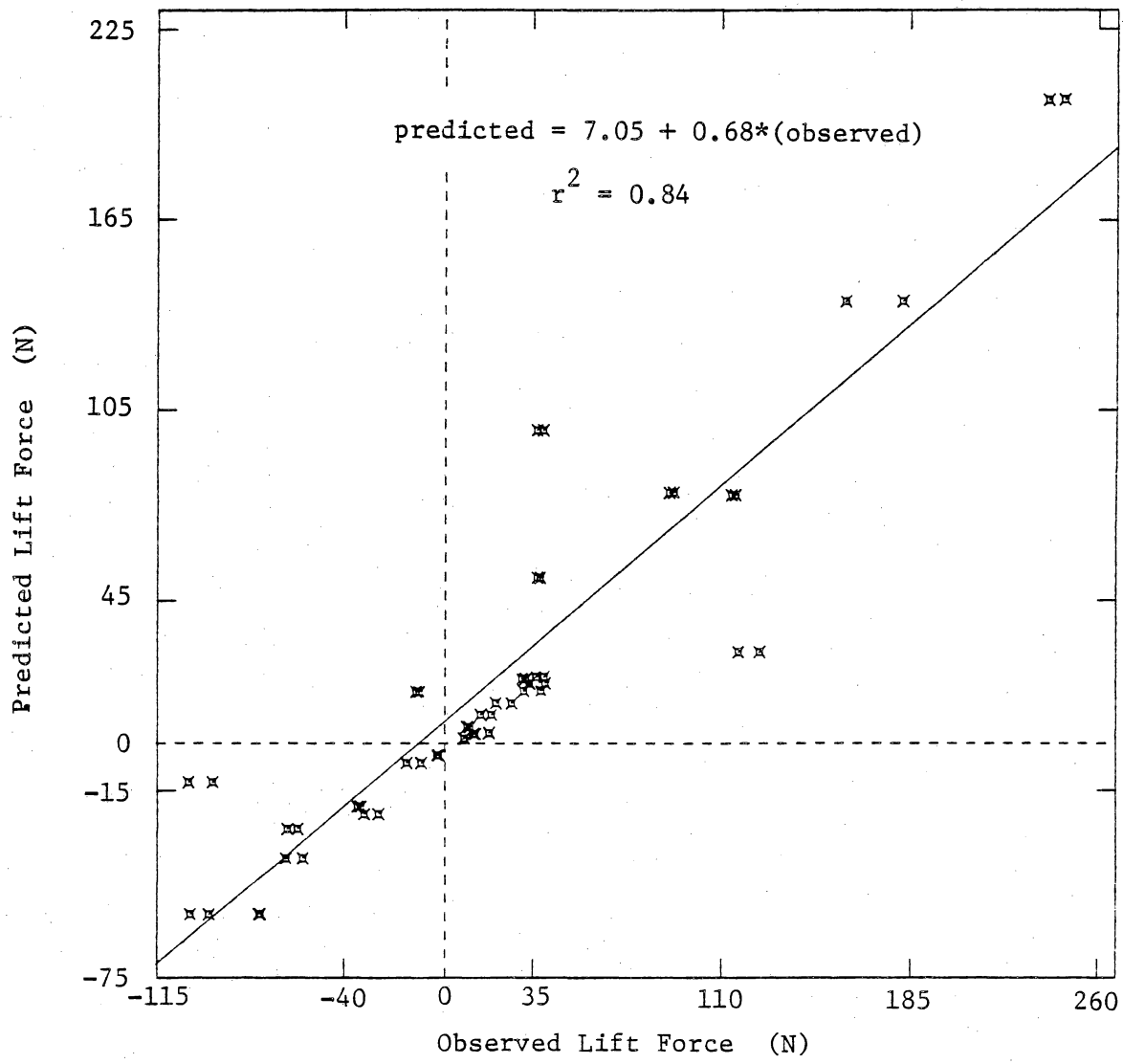

Figure 16 Comparison of predicted and experimentally observed lift force.

respectively at the 5 % level. The mean prediction error is 3.27 N.

The tool angle (β) was found to be the independent variable most significantly correlated with the lift force prediction error. The error is plotted against the tool angle in Figure 17. It can be seen that there is a definite negative correlation between the prediction error and tool angle. The correlation coefficient between the two is -0.53 which is significantly different from zero at the 1 % level. A possible reason for this tendency is that there may be some error in the relationship assumed between the tool angle and soil metal friction angle.

Figure 18 shows the prediction error for the vertical force plotted against tool speed. As with the draft force, no definite relationship is observed, with the correlation coefficient between the two being 0.14.

4.2.3 Dimensions of the failure wedge.

The predicted and measured values of rupture distance (r) and side wedge width (s) are presented in Table 2. The predicted values are those obtained from the soil-tool model for the wedge producing minimum resistance in each of the cases considered. The measured values are averages of the measurements taken for each combination of tool width, an-

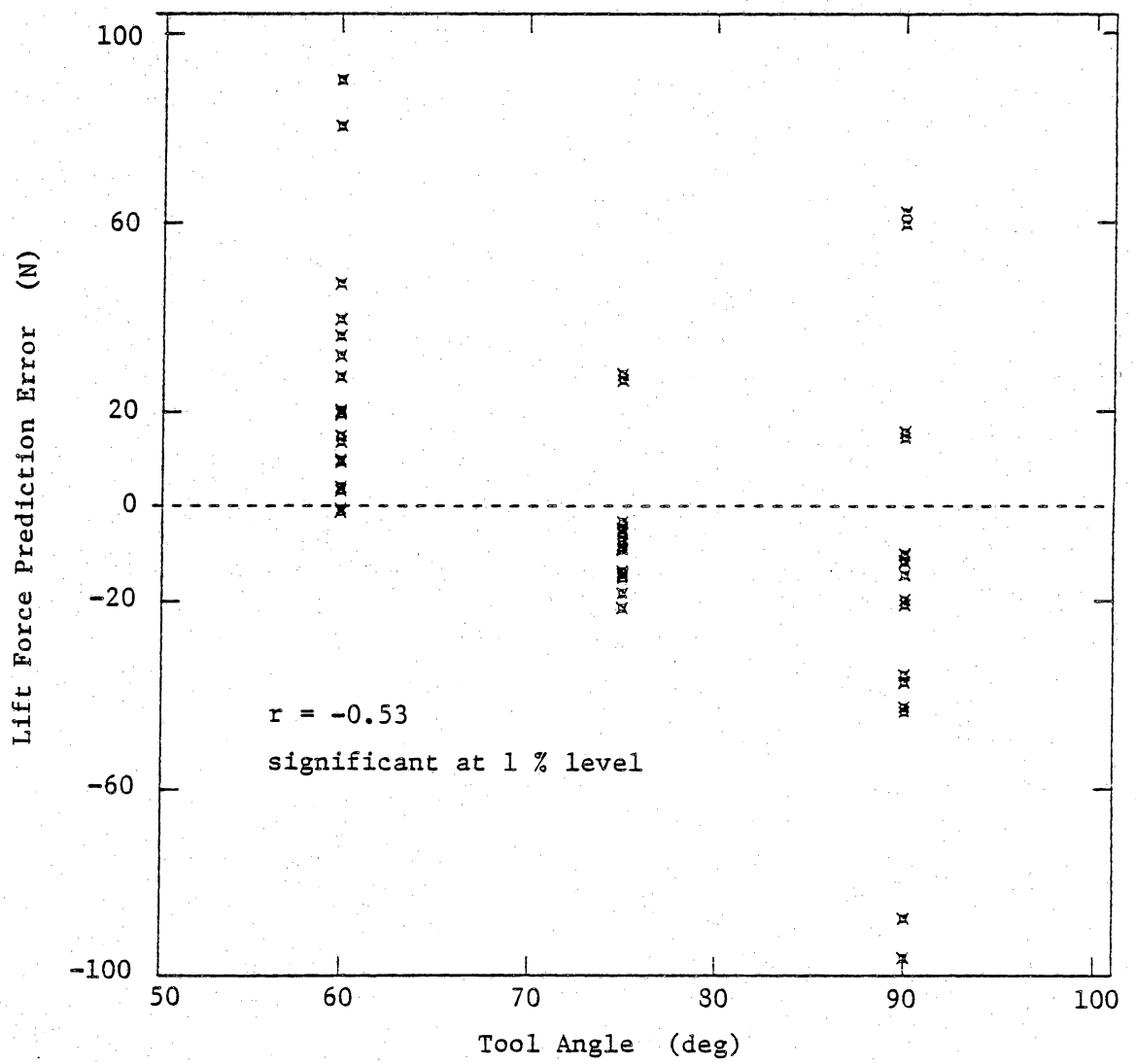

Figure 17 Effect of tool angle on lift force prediction error.

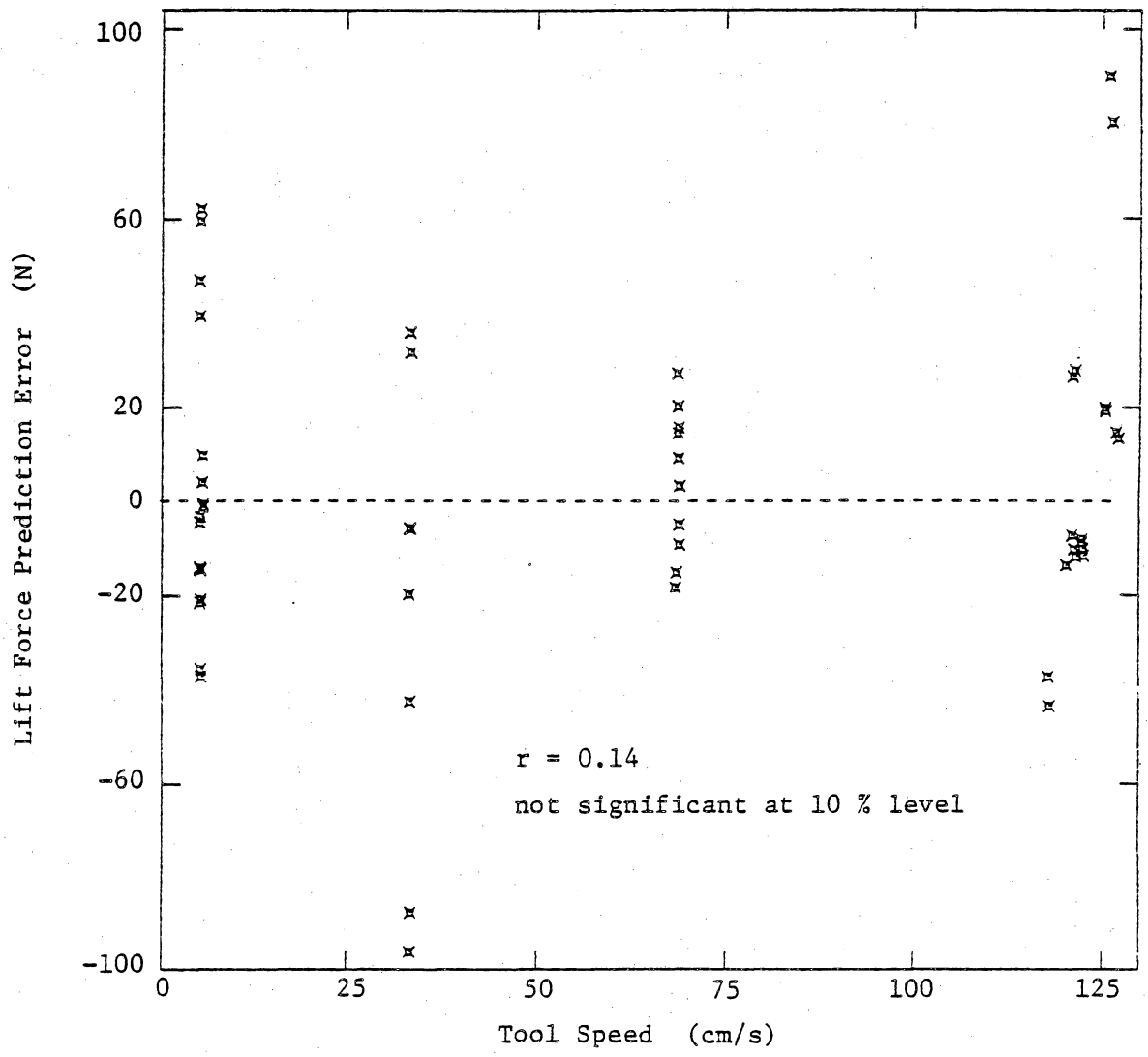

Figure 18 Effect of tool speed on lift force prediction error.

Table 2. Predicted and experimentally observed rupture distance and side wedge width for 36 soil bin tests.

Test Condition				Observed Values		Predicted Values	
B	β	D	V	r	s	r	s
(cm)	(deg)	(cm)	(cm/s)	(cm)	(cm)	(cm)	(cm)
2.5	60	5.1	5.7	10.4	4.2	10.4	4.1
2.5	60	5.1	5.7	10.4	4.2	10.4	4.1
2.5	60	10.2	126.8	15.9	6.6	20.9	8.7
2.5	60	10.2	127.2	15.9	6.6	20.9	8.7
2.5	60	15.2	68.8	20.6	9.1	29.7	12.6
2.5	60	15.2	68.7	20.6	9.1	29.7	12.6
5.1	60	5.1	68.9	10.5	4.5	11.3	4.5
5.1	60	5.1	68.8	10.5	4.5	11.3	4.5
5.1	60	15.2	125.3	22.5	9.9	31.9	13.5
5.1	60	15.2	125.4	22.5	9.9	31.9	13.5
7.6	60	10.2	5.6	18.5	8.1	21.7	9.1
7.6	60	10.2	5.6	18.5	8.1	21.7	9.1
10.2	60	5.1	125.9	10.6	4.1	12.6	5.1
10.2	60	5.1	126.2	10.6	4.1	12.6	5.1
10.2	60	10.2	33.2	18.4	7.1	22.4	9.4
10.2	60	10.2	33.3	18.4	7.1	22.4	9.4
10.2	60	15.2	5.3	23.3	10.2	32.1	13.6
10.2	60	15.2	5.2	23.3	10.2	32.1	13.6
2.5	90	5.1	122.6	8.3	5.6	11.7	7.7
2.5	90	5.1	122.4	8.3	5.6	11.7	7.7
2.5	90	10.2	68.8	14.8	8.4	20.7	11.7
2.5	90	10.2	68.8	14.8	8.4	20.7	11.7
2.5	90	15.2	5.4	16.4	9.4	29.1	15.3
2.5	90	15.2	5.4	16.4	9.4	29.1	15.3
5.1	90	5.1	5.4	11.6	7.7	11.4	7.6
5.1	90	5.1	5.4	11.6	7.7	11.4	7.6
5.1	90	10.2	121.5	17.6	11.0	22.9	12.6
5.1	90	10.2	121.2	17.6	11.0	22.9	12.6
7.6	90	15.2	33.2	25.4	14.0	31.5	16.4
7.6	90	15.2	33.1	25.4	14.0	31.5	16.4
10.2	90	5.1	33.4	15.2	9.5	12.2	7.9
10.2	90	5.1	33.3	15.2	9.5	12.2	7.9
10.2	90	10.2	5.5	22.7	12.6	22.4	12.4
10.2	90	10.2	5.4	22.7	12.6	22.4	12.4
10.2	90	15.2	118.0	28.6	14.8	34.6	17.8
10.2	90	15.2	117.9	28.6	14.8	34.6	17.8

gle, and depth. Figures 19 and 20 show the predicted values plotted against the observed values for r and s respectively. Regression equations for each plot are shown in the figures.

The prediction errors for r and s were found to be very highly correlated. This was expected, since s and r are highly correlated. Therefore, any observations made on the prediction error for r apply as well to the error for s.

In general, the model has a tendency to overpredict the rupture distances. The mean error on r is 4.5 cm and that on s is 1.9 cm. A possible reason for this tendency is the replacment of the actual curved rupture surface with a straight plane in the model. Figure 21 shows that the predicted failure surface creates a greater rupture distance.

Further analysis showed significant correlation between rupture distance prediction error and the depth-width ratio. Figure 22 shows the error plotted against the D/B ratio. The correlation coefficient between the two is 0.71 which is signifigant at the 1 % level. The maximum underprediction and overprediction are at the low and high depth-width ratios respectively. The draft force prediction error shows the same trend. Thus, as stated previously, it is likely that the maximum underpredictions and overpredictions in draft force are at least partially due to the similar prediction errors in the size of the wedge.

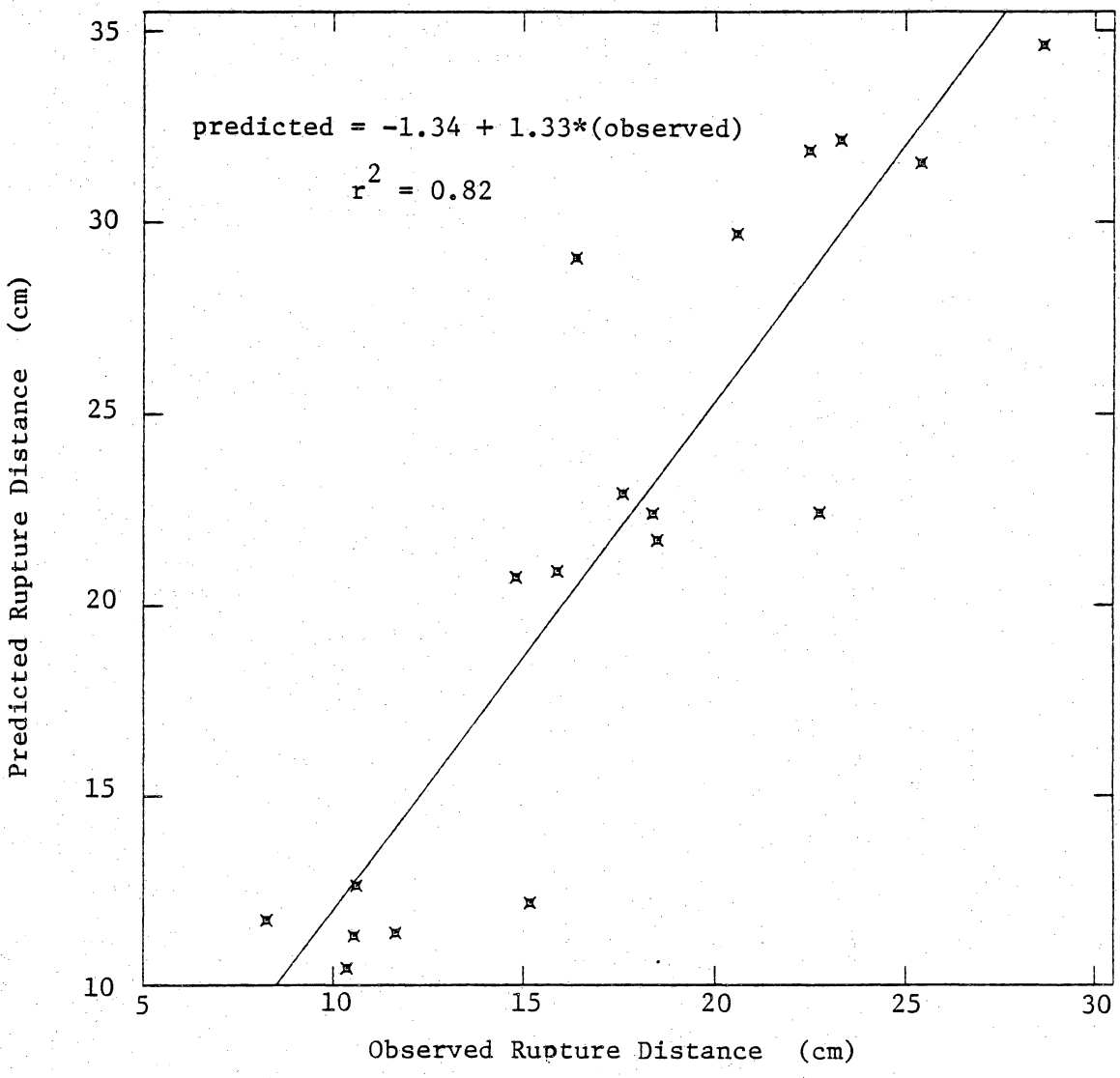

Figure 19 Comparison of predicted and experimentally observed rupture distance.

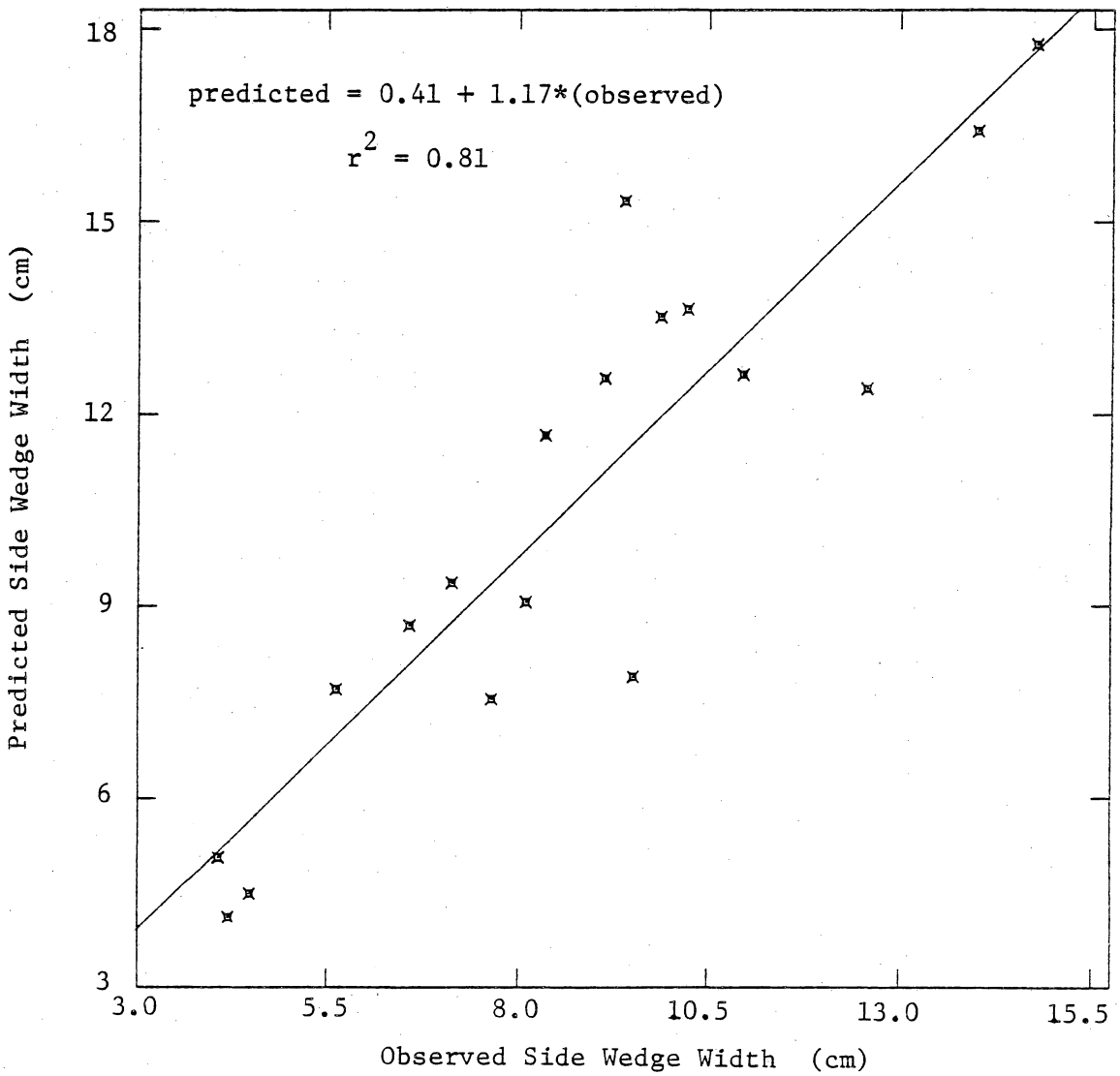

Figure 20 Comparison of predicted and experimentally observed side wedge width.

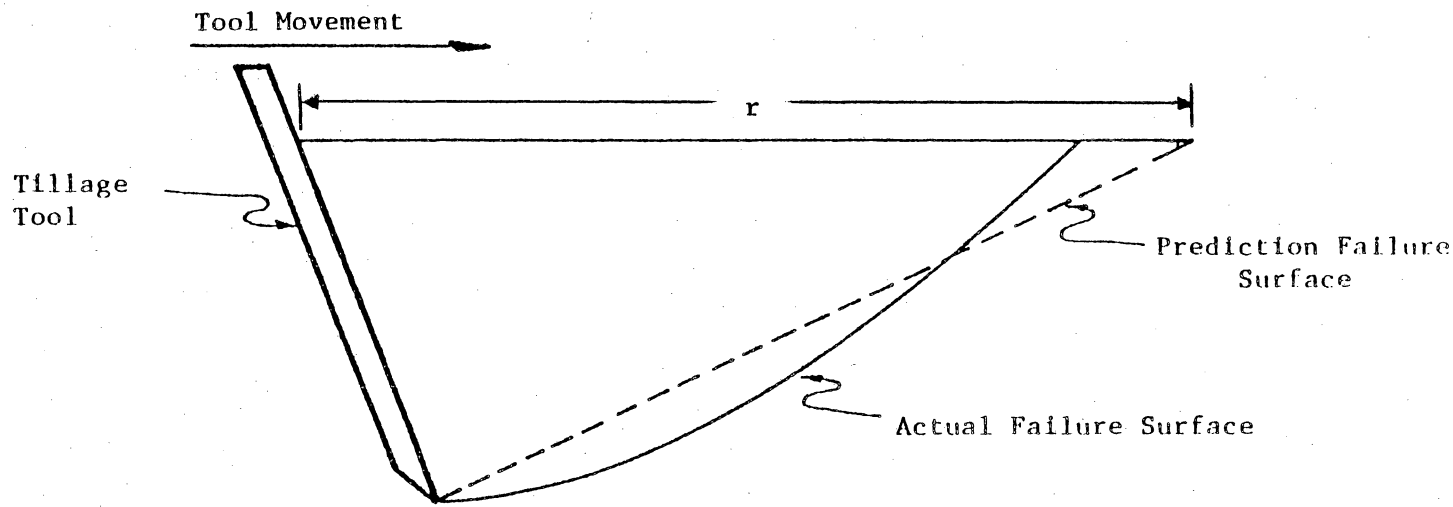

Figure 21 Comparison of predicted and observed failure surfaces.

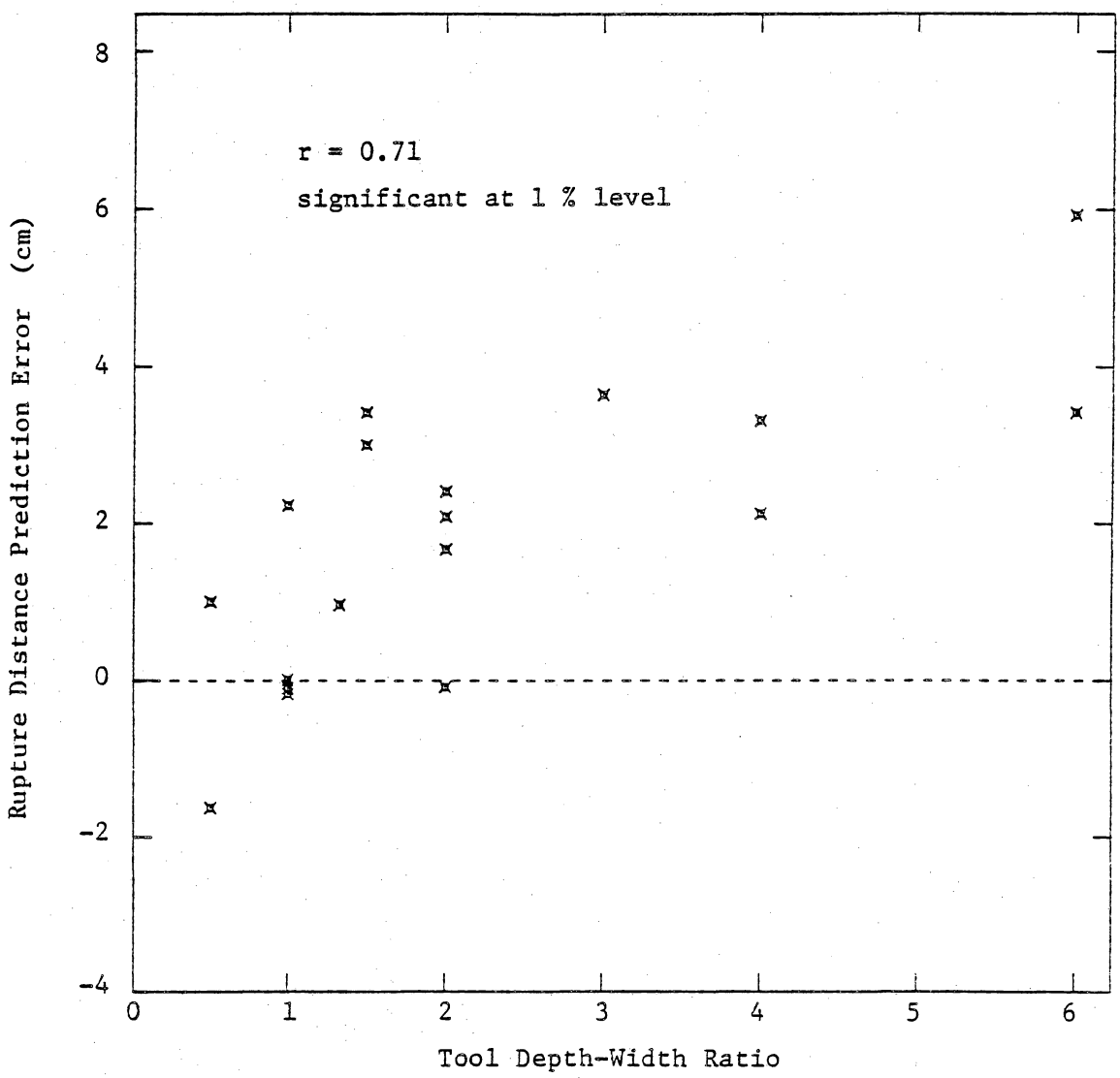

Figure 22 Effect of tool depth-width ratio on rupture distance prediction error.

The inability of the model to adequately predict the size of the failure wedge at the low and high depth-width ratios, may be a result the failure wedge changing form at the two extremes. The tool operating at the low depth ratio of 0.5 is considered "shallow" according to O'Callaghan and Farrelly (1964) and "wide" by Payne (1956). O'Callaghan and Farrelly consistently observed a change in soil-tool interaction at a critical depth-width ratio between 0.5 and 1.

The large overpredictions of rupture distance at the high depth-ratio of 6 may be a result of the phenomenon observed by Godwin and Spoor (1977). For a deep-working tine, they observed a critical depth along the tool from which point a rupture surface developed forward and upward to the soil surface. Ahead of the tool below the critical depth, soil appeared to move forward with no definite shear plane being formed. The model developed in the present study considers that for all tool depths, the rupture surface develops from the lower tip of the tool and not from some intermediate depth along the tool. Thus, if the model considers the rupture surface to be initiated at a point lower than actual, the rupture distance at the soil surface will be overpredicted.

Figure 23 shows no definite relationship between the rupture distance prediction error and tool speed. The same is

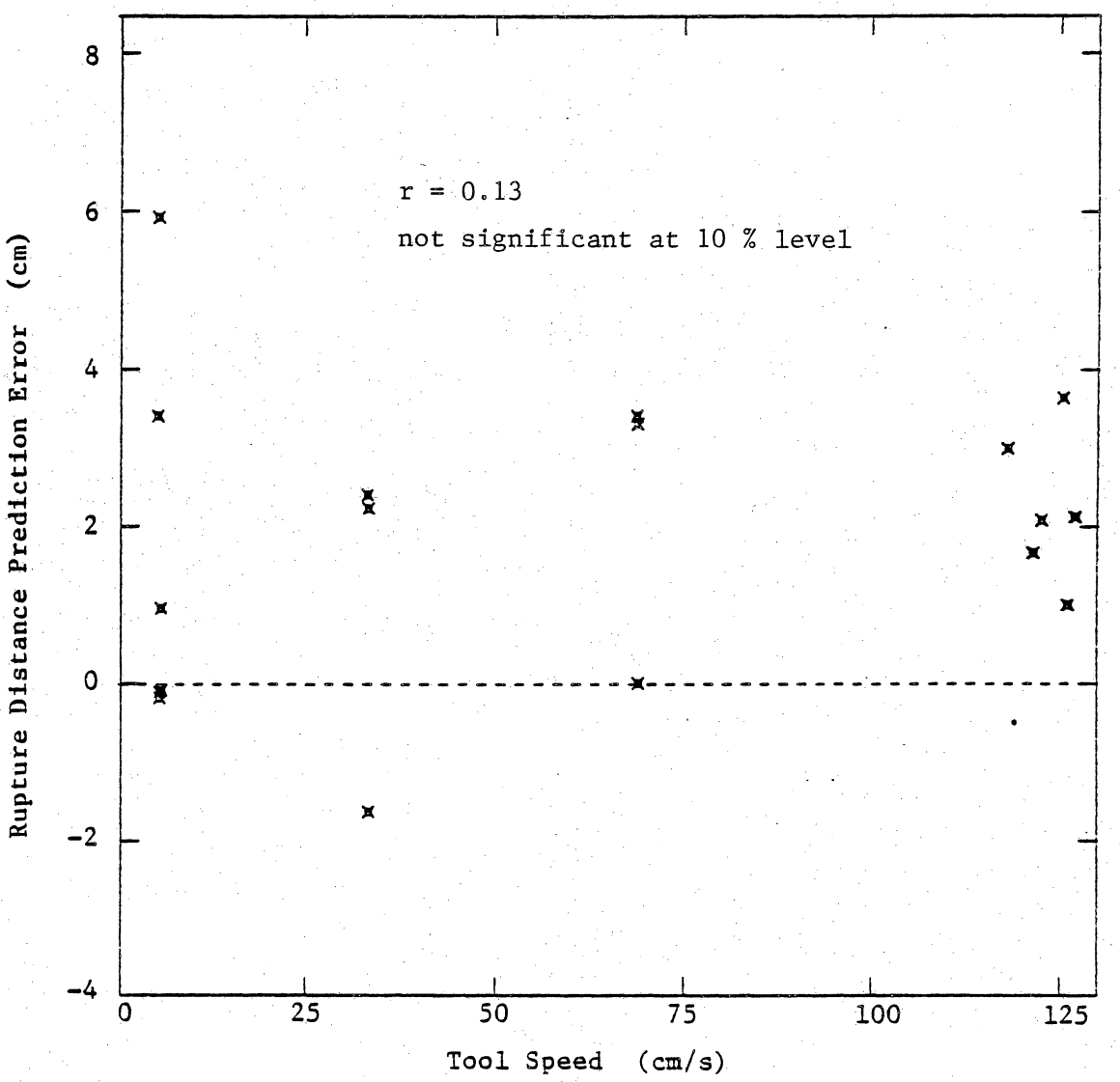

Figure 23 Effect of tool speed on rupture distance prediction error.

true for the side wedge width. This suggests that inclusion in the model of the relationship between s, r, and β developed at low tool speeds is valid.

4.2.4 Location of resultant force.

The depth from the undisturbed soil surface to the point of intersection between the total resultant force and the tool (D_t) was calculated from FX, FZ, and MY for each soil bin test. The values determined for D_t, as well as values for the ratio between the resultant force depth and the tool depth (D_t/D), are presented in Table A-4. Passive Earth Pressure Theory predicts the D_t/D ratio to be between one-half and two-thirds. The average ratio calculated is 0.50, and there is considerable scatter in the calculated values, with some negative and some greater than one. However, the majority of the depth ratios lie between one-fourth and three-fourths, which would be reasonable values.

A strong correlation was found between the D_t/D ratio and tool speed (Figure 24). The correlation coefficient between the two is -0.55 which is significant at the 1 % level. It is possible that the high D_t/D ratios at the low tool speed are a result of higher soil compression taking place near the bottom of the tool. At the same time, this soil compression by the tool may not be significant at the high speed and a different type of soil failure may take place.

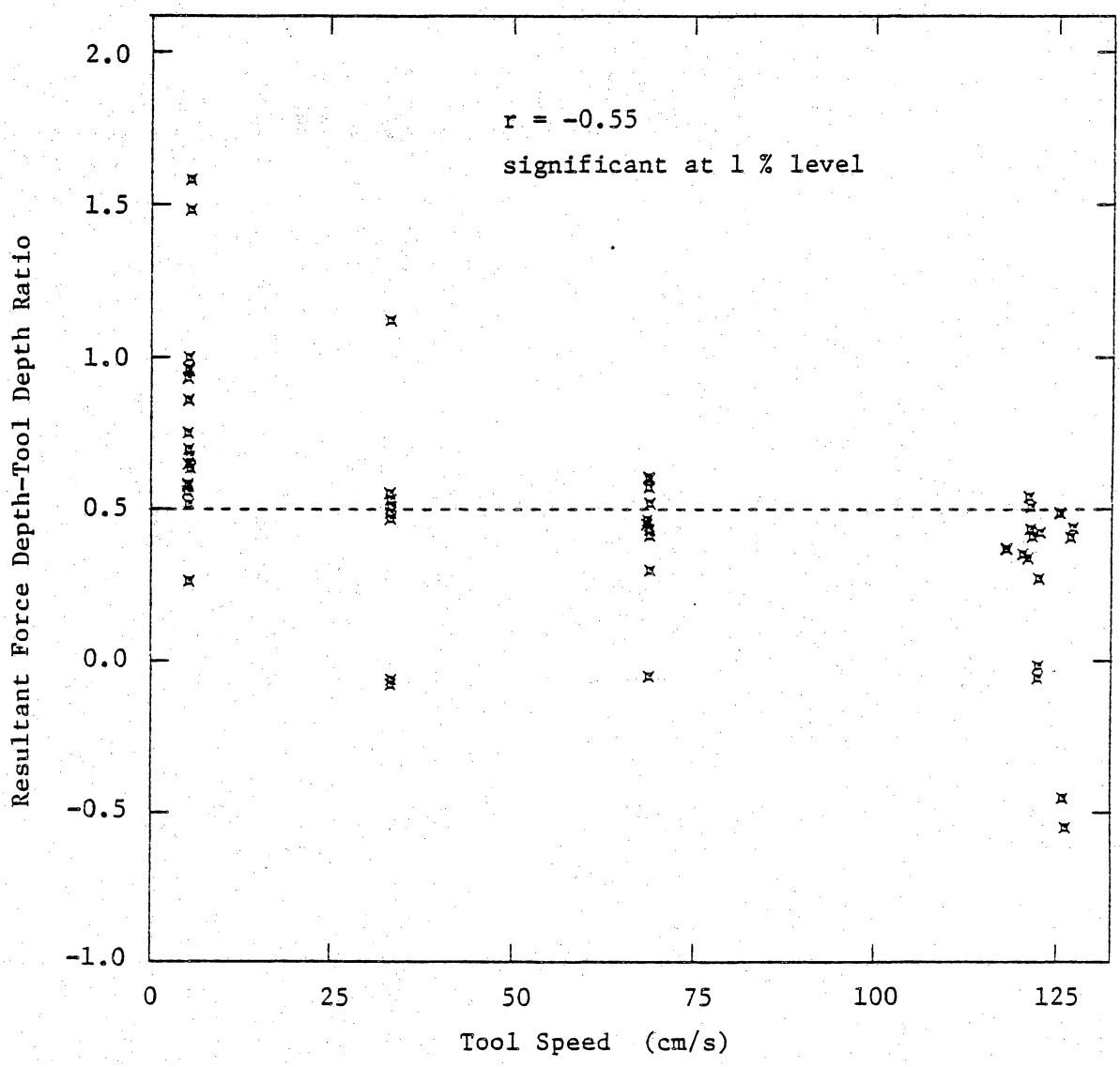

Figure 24 Effect of tool speed on resultant force depth-tool depth ratio.

It is interesting to note that the D_t/D ratio was found to be highly correlated with tool speed, while the forces and wedge dimensions were found to be independent of speed. These types of observations clearly show how complex the speed effect is on soil-tillage tool interaction.

Chapter V

CONCLUSIONS

1. The angle of internal friction, soil-metal friction angle, cohesion and adhesion were found to be independent of shear rate for an artificial soil tested.
2. A soil-tillage tool interaction model developed for quasi-static soil failure was modified to include dynamic effects. The model gave reasonable predictions of tool forces encountered by narrow flat tools.
3. The model demonstrated that terms including accelerational force effects can account for a large portion of the increase in tool force observed to occur with an increase in tool speed.

LITERATURE CITED

Aref, K. E., W. J. Chancellor and D. R. Nielson. 1975. Dynamic shear strength properties of unsaturated soils. Trans. ASAE, 18(5):818-823.

Cline, B. E. and J. V. Perumpral. 1982. A general purpose, microcomputer based data acquisition system. ASAE Paper No. 82-5518. Am. Soc. Agric. Eng., St. Joseph, MI.

Cochran, W. G. and G. M. Cox. 1957. Experimental Designs. John Wiley and Sons, Inc., New York, NY.

Durant, D. M. 1979. Soil bin test facility for soil-tillage tool interaction studies. Masters thesis, Va. Poly. Inst. and State Univ., Blacksburg, VA.

Durant, D. M., J. V. Perumpral and C. S. Desai. 1981. Soil bin test facility for soil-tillage tool interaction studies. Soil and Tillage Res., 1(3):289-298.

Flenniken, J. M., R. E. Hefner, and J. A. Weber. 1977. Dynamic soil strength parameters from unconfined compression tests. Trans. ASAE, 20(1):21-25.

Gill, W. R. and G. E. Vanden Berg. 1968. Soil dynamics in tillage and traction. Agric. Res. Serv., Washington, DC.

Godwin, R. J. and G. Spoor. 1977. Soil failure with narrow tines. J. Agric. Eng. Res., 22(3):213-228.

Grisso, R. D. 1980. A soil-tool interaction model for narrow tillage tools. Masters thesis, Va. Poly. Inst. and State Univ., Blacksburg, VA.

Hettiaratchi, D. P. and A. R. Reece. 1967. Symmetrical three-dimensional soil failure. J. Terramech., 4(3):45-67.

Hettiaratchi, D. P. and A. R. Reece. 1974. The calculation of passive soil resistance. Geotechnique, 24(3):289-310.

Hettiaratchi, D. P., B. D. Witney and A. R. Reece. 1966. The calculation of passive pressure in two-dimensional soil failure. J. Agric. Eng. Res., 11(2):89-107.

Koopmans, L. H. 1981. An introduction to contemporary statistics. Duxburry Press, Belmont, CA.

McKyes, E. 1978. The calculation of draft forces and soil failure boundaries of narrow cutting blades. Trans. ASAE, 21(1):20-24.

McKyes, E. and O. S. Ali. 1977. The cutting of soil by narrow blades. J. Terramech., 14(2):43-58.

Meyerhof, G. C. 1951. The ultimate bearing capacity of foundations. Geotechnique, 2(4):310-332.

O,Callaghan, J. R. and K. M. Farelly. 1964. Cleavage of soil by tined implements. J. Agric. Eng. Res., 9(3):259-270.

Ohde, J. 1938. Theory of soil pressure with particular reference to its distribution. Die Bautechnik, 16:150, 176, 241, 331, 480, 570, 753.

Osman, M. S. 1964. The mechanics of soil cutting blades. J. Agric. Eng. Res., 9(4):313-328.

Payne, P. C. J. 1956. The relationship between the mechanical properties of soil and the performance of simple cultivation implements. J. Agric. Eng. Res., 1(1):23-50.

Payne, P. C. J. and D. W. Tanner. 1959. The relationship between rake angle and the performance of simple cultivation implements. J. Agric. Eng. Res., 4(4):312-325.

Perumpral, J. V., R. D. Grisso and C. S. Desai. 1983. A soil-tool model based on limit equilibrium analysis. Trans. ASAE, 26(4):991-995.

Pradtl, L. 1920. The hardness of plastic bodies. Nachr. Kgl. Ges. Wiss. Gottingen, Math. Phys. Klasse.

Reece, A. R. 1965. The fundamental equation of earth-moving mechanics. Proc. Symp. Earthmoving Machinery, Inst. Mech. Engrs. 179, Pt. 3E.

Rowe, R. J. and K. K. Barnes. 1961. Influence of speed on elements of draft of a tillage tool. Trans. ASAE, 4(1):55-57.

Siemens, J. C., J. A. Weber and T. H. Thorburn. 1965. Mechanics of soil as influnced by model tillage tools. Trans. ASAE, 8(1):1-7.

Soehne, W. H. 1956. Some Principles of soil mechanics as applied to agricultural engineering. Grundlagen der Landtechnik, 7:11-27.

Stafford, J. V. 1979. The performance of a rigid tine in relation to soil properties and speed. J. Agric. Eng. Res., 24(1):41-55.

Stafford, J. V. and D. W. Tanner. 1983a. Effect of rate on soil shear strength and soil-metal friction. I. Shear strength. Soil and Tillage Res., 3(3):245-260.

Stafford, J. V. and D. W. Tanner. 1983b. Effect of rate on soil shear strength and soil-metal friction. II. Soil-metal friction. Soil and Tillage Res., 3(4):321-330.

Sture, S., C. S. Desai and J. V. Perumpral. 1980. Laboratory behavior of an artificial soil. Report No. VPI-E 80.12. Va. Poly. Inst. and State Univ., Blacksburg, VA.

Terzahgi, K. 1943. Theoretical soil mechanics. John Wiley and Sons, Inc., New York, NY.

Turnage, G. W. and D. R. Freitag. 1970. Effects of cone velocity and size on soil penetration resistance. ASAE Paper No. 69-670. Am. Soc. Agric. Eng., St. Joseph, MI.

Wismer, R. D. and H. J. Luth. 1972. Rate effects in soil cutting. J. Terramech., 8(3):11-21.

Appendix A

EXPERIMENTAL TEST DATA.

Table A-1. Rupture distance (r) and maximum side wedge width (s) values measured at different combinations of tool width, angle, and depth.

Tool Width B (cm)	Tool Angle β (deg)	Tool Depth D (cm)	Rupture Distance r (cm)	Side Wedge Width s (cm)
2.5	60	5.1	8.3	4.0
2.5	60	5.1	12.1	4.4
2.5	60	5.1	10.5	4.1
2.5	60	5.1	10.2	4.4
2.5	60	5.1	10.8	4.0
2.5	60	10.2	15.2	6.5
2.5	60	10.2	16.5	6.4
2.5	60	10.2	16.5	7.0
2.5	60	10.2	15.9	6.3
2.5	60	10.2	15.2	7.0
2.5	60	15.2	20.3	8.9
2.5	60	15.2	21.6	9.2
2.5	60	15.2	21.0	9.2
2.5	60	15.2	18.4	8.9
2.5	60	15.2	21.6	9.5
5.1	60	5.1	10.2	4.6
5.1	60	5.1	10.5	4.9
5.1	60	5.1	11.1	4.6
5.1	60	5.1	10.2	4.4
5.1	60	5.1	10.8	3.8
5.1	60	10.2	17.1	5.7
5.1	60	10.2	17.8	6.4
5.1	60	10.2	18.1	6.7
5.1	60	10.2	17.1	6.5
5.1	60	10.2	17.5	6.5
5.1	60	15.2	21.6	9.7
5.1	60	15.2	22.9	9.8
5.1	60	15.2	23.2	9.5
5.1	60	15.2	22.9	10.2
5.1	60	15.2	21.9	10.2
7.6	60	5.1	11.4	4.4
7.6	60	5.1	11.4	4.1
7.6	60	5.1	11.4	4.4
7.6	60	5.1	10.8	4.4
7.6	60	5.1	11.1	4.3
7.6	60	10.2	17.8	8.3
7.6	60	10.2	18.4	8.1
7.6	60	10.2	18.4	7.9
7.6	60	10.2	18.1	8.6

Table A-1. (continued)

Tool Width B	Tool Angle β	Tool Depth D	Rupture Distance r	Side Wedge Width s
(cm)	(deg)	(cm)	(cm)	(cm)
7.6	60	10.2	19.7	7.6
7.6	60	15.2	26.0	10.5
7.6	60	15.2	27.9	10.2
7.6	60	15.2	26.4	10.2
7.6	60	15.2	26.0	10.0
7.6	60	15.2	26.0	10.2
10.2	60	5.1	10.2	4.4
10.2	60	5.1	10.5	3.8
10.2	60	5.1	10.8	3.8
10.2	60	5.1	10.8	4.1
10.2	60	5.1	10.8	4.1
10.2	60	10.2	17.8	7.0
10.2	60	10.2	18.4	6.7
10.2	60	10.2	18.4	7.1
10.2	60	10.2	18.7	7.5
10.2	60	10.2	18.4	7.3
10.2	60	15.2	22.9	10.5
10.2	60	15.2	24.1	10.2
10.2	60	15.2	22.5	9.2
10.2	60	15.2	23.5	10.5
10.2	60	15.2	23.5	10.8
2.5	90	5.1	8.9	5.7
2.5	90	5.1	7.9	5.0
2.5	90	5.1	8.3	5.6
2.5	90	5.1	7.6	6.4
2.5	90	5.1	8.6	5.4
2.5	90	10.2	14.6	7.1
2.5	90	10.2	14.9	9.0
2.5	90	10.2	14.6	8.9
2.5	90	10.2	14.0	8.3
2.5	90	10.2	15.9	8.4
2.5	90	15.2	16.5	9.2
2.5	90	15.2	16.5	10.2
2.5	90	15.2	16.5	9.0
2.5	90	15.2	16.2	9.2
2.5	90	15.2	16.2	9.4
5.1	90	5.1	11.4	7.5
5.1	90	5.1	11.4	7.5
5.1	90	5.1	11.4	7.6
5.1	90	5.1	11.7	8.1
5.1	90	5.1	12.1	7.6

Table A-1. (continued)

Tool Width B (cm)	Tool Angle β (deg)	Tool Depth D (cm)	Rupture Distance r (cm)	Side Wedge Width s (cm)
5.1	90	10.2	16.5	10.3
5.1	90	10.2	17.5	11.1
5.1	90	10.2	17.8	11.1
5.1	90	10.2	17.8	10.2
5.1	90	10.2	18.4	12.1
5.1	90	15.2	20.0	12.1
5.1	90	15.2	22.2	12.4
5.1	90	15.2	21.3	12.4
5.1	90	15.2	19.4	12.4
5.1	90	15.2	22.2	12.2
7.6	90	5.1	14.0	8.7
7.6	90	5.1	14.0	8.9
7.6	90	5.1	14.0	8.9
7.6	90	5.1	13.7	8.9
7.6	90	5.1	13.7	8.6
7.6	90	10.2	20.3	11.1
7.6	90	10.2	21.3	11.7
7.6	90	10.2	21.3	12.1
7.6	90	10.2	21.6	12.1
7.6	90	10.2	21.0	12.2
7.6	90	15.2	24.1	13.7
7.6	90	15.2	25.4	13.8
7.6	90	15.2	25.4	13.3
7.6	90	15.2	26.0	14.6
7.6	90	15.2	26.0	14.6
10.2	90	5.1	15.2	9.2
10.2	90	5.1	14.9	9.7
10.2	90	5.1	14.9	9.7
10.2	90	5.1	15.2	9.4
10.2	90	5.1	15.6	9.7
10.2	90	10.2	21.6	12.4
10.2	90	10.2	22.2	12.7
10.2	90	10.2	23.4	12.0
10.2	90	10.2	23.5	12.9
10.2	90	10.2	22.5	12.9
10.2	90	15.2	28.6	13.8
10.2	90	15.2	27.6	14.8
10.2	90	15.2	27.9	14.9
10.2	90	15.2	28.6	14.9
10.2	90	15.2	30.5	15.4

Table A-2. Normal stress and shear stress values from direct shear test on the artificial soil at three shear rates.

Shear Rate	Normal Stress σ	Shear Stress τ
(cm/min)	(N/cm^2)	(N/cm^2)
0.5	0.77	0.81
0.5	0.77	0.76
0.5	1.41	1.19
0.5	1.41	1.25
0.5	1.97	1.67
0.5	1.97	1.62
50.8	0.77	0.76
50.8	0.77	0.75
50.8	1.41	1.28
50.8	1.41	1.29
50.8	1.97	1.60
50.8	1.97	1.67
127.0	0.77	0.78
127.0	0.77	0.79
127.0	1.41	1.30
127.0	1.41	1.29
127.0	1.97	1.69
127.0	1.97	1.70

Table A-3. Normal stress and shear stress values from soil-metal friction tests on the artificial soil at three shear rates.

Shear Rate	Normal Stress σ'	Shear Stress τ'
(cm/min)	(N/cm^2)	(N/cm^2)
0.5	2.70	1.37
0.5	2.70	1.37
0.5	2.70	1.29
0.5	7.46	3.26
0.5	7.46	3.54
0.5	7.46	3.41
0.5	11.77	5.41
0.5	11.77	5.25
0.5	11.77	5.19
50.8	2.70	1.38
50.8	2.70	1.40
50.8	7.46	3.45
50.8	7.46	3.51
50.8	11.77	5.34
50.8	11.77	5.30
12.70	2.70	1.39
12.70	2.70	1.42
12.70	7.46	3.66
12.70	7.46	3.40
12.70	11.77	5.52
12.70	11.77	5.38

Table A-4. Depth of the total resultant tool force, and the ratio of this depth to the tool depth, for 54 soil bin tests.

Tool Width B	Tool Angle β	Tool Depth D	Tool Speed V	Total Force Depth D_t	Depth Ratio D_t/D
(cm)	(deg)	(cm)	(cm/s)	(cm)	
2.5	60	5.1	5.7	8.0	1.58
2.5	60	5.1	5.7	7.5	1.48
2.5	75	10.2	5.4	8.7	0.86
2.5	75	10.2	5.3	9.8	0.96
2.5	90	15.2	5.4	10.6	0.70
2.5	90	15.2	5.4	9.9	0.65
5.1	90	5.1	5.4	5.1	1.00
5.1	90	5.1	5.4	4.9	0.96
7.6	60	10.2	5.6	6.9	0.67
7.6	60	10.2	5.6	6.4	0.63
7.6	75	15.2	5.3	8.8	0.58
7.6	75	15.2	5.3	8.8	0.58
10.2	60	15.2	5.3	8.9	0.58
10.2	60	15.2	5.2	8.5	0.56
10.2	75	5.1	5.3	3.8	0.75
10.2	75	5.1	5.3	4.7	0.93
10.2	90	10.2	5.5	2.7	0.26
10.2	90	10.2	5.4	5.2	0.52
2.5	75	5.1	33.2	2.7	0.53
2.5	75	5.1	33.3	5.7	1.12
7.6	90	15.2	33.2	7.4	0.49
7.6	90	15.2	33.1	8.4	0.55
10.2	60	10.2	33.2	4.8	0.47
10.2	60	10.2	33.3	5.2	0.51
10.2	90	5.1	33.4	-0.3	-0.06
10.2	90	5.1	33.3	-0.4	-0.08
2.5	60	15.2	68.8	9.1	0.60
2.5	60	15.2	68.7	9.2	0.61

Table A-4. (continued)

Tool Width B	Tool Angle β	Tool Depth D	Tool Speed V	Total Force Depth D_t	Depth Ratio D_t/D
(cm)	(deg)	(cm)	(cm/s)	(cm)	
2.5	90	10.2	68.8	5.8	0.57
2.5	90	10.2	68.8	5.3	0.52
5.1	60	5.1	68.9	1.5	0.30
5.1	60	5.1	68.8	-0.3	-0.05
7.6	75	10.2	68.8	4.4	0.43
7.6	75	10.2	68.8	4.2	0.41
10.2	75	15.2	68.5	7.1	0.47
10.2	75	15.2	68.7	6.9	0.45
2.5	60	10.2	126.8	4.1	0.41
2.5	60	10.2	127.2	4.5	0.44
2.5	75	15.2	121.3	7.7	0.51
2.5	75	15.2	121.0	8.2	0.54
2.5	90	5.1	122.6	2.2	0.42
2.5	90	5.1	122.4	1.4	0.27
5.1	60	15.2	125.3	7.4	0.49
5.1	60	15.2	125.4	7.4	0.49
5.1	75	5.1	122.4	-0.1	-0.02
5.1	75	5.1	122.3	-0.3	-0.06
5.1	90	10.2	121.5	4.2	0.41
5.1	90	10.2	121.2	4.4	0.44
10.2	60	5.1	125.9	-2.3	-0.45
10.2	60	5.1	126.2	-2.8	-0.55
10.2	75	10.2	120.2	3.6	0.35
10.2	75	10.2	121.0	3.4	0.34
10.2	90	15.2	118.0	5.6	0.37
10.2	90	15.2	117.9	5.6	0.37

The vita has been removed from the scanned document